

Optical control of neocortical circuits to probe how connectivity influences behavioural salience



James Rowland

Corpus Christi College

University of Oxford

A thesis submitted for the degree of

Doctor of Philosophy

Trinity 2021

Acknowledgements

Abstract

The brains of higher organisms are composed of anatomically and functionally distinct regions performing specialised tasks. However, individual regions do not operate in isolation. Hence, the orchestration of complex behaviours requires communication between brain regions and reliable transmission of information between them. In this thesis I explore how we can study this process directly by generating neural activity that propagates between brain regions and drives behaviour, allowing me to assess how populations of neurons in sensory cortex act in concert to transmit information. I achieved this by imaging two hierarchically organised and densely interconnected regions, the primary and secondary somatosensory cortex (S1 and S2) in mice while performing two-photon photostimulation of S1 neurons and assigning behavioural salience to the photostimulation. I found that the probability of perception is determined by both the variance of the S1 network and the strength of the photostimulation. Conceptually this means that maximising the signal-to-noise ratio of an incoming stimulus is critical to its continued propagation downstream. Further, I show that propagated, behaviourally salient activity elicits balanced, persistent and generalised activation of the downstream region, consistent with inhibitory stabilised network models with dense recurrent connectivity. Hence, my work adds to existing understanding of cortical function by identifying how population activity is formatted to ensure robust transmission of information, allowing specialised brain regions to communicate and coordinate behaviour.

Summary of contributions

I declare that this thesis is my own and that attribution has been given where information was derived from other sources. Aside from the exceptions outlined below, I conceptualised the project, designed and assembled the equipment, performed the experiments, analysed the data and constructed all figures. While all writing contained herein is my own, the project as a whole has relied on key contributions from others. Throughout, the text uses the pronoun 'We' indicating myself and the team below.

Josh Keeling: Collection of ~50% of the two-photon behavioural data (under supervision from myself).

Robert Lees: Performed ~50% of the surgeries used to collect two-photon behavioural data.

Thijs van der Plas, Matthias Loidolt, Jonas Dehning, Viola Priesemann: Assistance with data analysis, particularly logistic regression classifiers.

Adam Packer: Conceptualisation of the project and supervision throughout.

Contents

List of Figures	8
1 Introduction	9
1.1 Recording neural activity	12
1.2 Manipulating neural activity with light	14
1.3 All-optical interrogation of neural circuits <i>in vivo</i>	16
1.4 Somatosensory cortex as a model system	17
1.5 Primary and secondary somatosensory cortex	18
1.6 Propagating neural activity	19
1.7 Driving behaviour directly through cortical stimulation	20
1.8 Summary	23
2 Driving behaviour with optogenetics	24
2.1 One-photon photostimulation	25
2.2 Two-photon photostimulation	29
3 All-optical control of neural circuits across brain regions	32
3.1 Localisation of S1 and S2	32
3.2 Simultaneous two-photon calcium imaging and photostimulation . .	34
4 Statistical modelling of evoked neural activity	39
4.1 The structure of evoked activity in S1 and S2	39
4.2 Perceived photostimulation elicit persistent activity in both S1 and S2 populations	46
4.3 Pre-stimulus population in S1 predicts the upcoming trial outcome	51
5 Discussion	55

5.1	E/I balance	57
5.2	Stimulus generalisation	58
5.3	Signal-to-noise ratio	59
5.4	Futher work	61
6	Materials and Methods	63
6.1	Animal usage	63
6.2	Surgical Procedures	64
6.3	Two-photon imaging	65
6.4	Widefield imaging	65
6.5	Two-photon optogenetic stimulation	66
6.6	Behavioural training	67
	One-photon behavioural training	69
	Two-photon behavioural training	70
6.7	Imaging Data analysis	71
6.8	Pre-stimulus population metrics	73
6.9	Normalisation and sorting of post-stimulus neural activity	74
6.10	Logistic regression classifiers	74
6.11	Behavioural data analysis	76
6.12	Statistical procedures	76

List of Figures

1	One-photon behavioural training.	28
2	Two-photon behavioural training.	31
3	Widefield localisation of S1 and S2	33
4	Two-photon calcium imaging and photostimulation	36
5	All-optical interrogation across brain regions	38
6	Structure of evoked activity in S1 and S2	41
7	Fraction of cells responding and grand average traces of all trial types in S1 and S2	43
8	Trial averaged raster plots for all sessions and trial types	44
9	Trial averaged raster plots for all sessions and trial types: continued	45
10	Perceived photostimuli elicit persistent activity in both S1 and S2 populations.	47
11	Dynamic decoders of individual sessions	48
12	Dynamic decoders of all trial types	50
13	Pre-stimulus population in S1 predicts the upcoming trial outcome	53
14	Further population metrics of pre-stimulus activity	54

“Between stimulus and response there is a space. In that space is our power to choose our response. In our response lies our growth and our freedom.”

– Viktor E. Frankl

1

Introduction

Contents

1.1	Recording neural activity	12
1.2	Manipulating neural activity with light	14
1.3	All-optical interrogation of neural circuits in vivo	16
1.4	Somatosensory cortex as a model system	17
1.5	Primary and secondary somatosensory cortex	18
1.6	Propagating neural activity	19
1.7	Driving behaviour directly through cortical stimulation	20
1.8	Summary	23

Key to the orchestration of behaviour by neural systems is that information, in the form of neural activity, is reliably and accurately transmitted between anatomically distinct brain regions performing specialised tasks. Activity is transformed at each stage of its journey, and circuits often perform multiple tasks in parallel^{1,2}, so it is challenging to disentangle which facets of neural activity contribute to a specific behaviour or process. In-depth analysis of cellular resolution recordings of neural activity during sensory stimulation^{3–7} and/or well-characterised behaviour^{8–12} has begun to disentangle how the sensory world, decisions and actions are encoded in individual brain regions. However, how activity is structured in order to facilitate its journey through the brain is less well understood. It is especially critical that

close attention is paid to unravelling how activity is propagated through the healthy brain, as dysfunction of this process is thought to play a key role in the aetiology of Alzheimer's disease^{13,14}, Parkinson's disease¹⁵ and epilepsy¹⁶.

For researchers studying streams of sensory processing, it is advantageous to circumvent the transformations of neural activity occurring at regions upstream from the brain region under study. This can be achieved by taking experimental control of neural activity and driving spikes directly through stimulation of individual neurons^{17–19} or groups of neurons^{20–24}. The recent renaissance in optical methods enables this to be achieved with unparalleled precision and flexibility. Specifically, two-photon optogenetics enables researchers to drive a predefined number of spikes in between one and hundreds of neurons with near single-cell precision, with the identities and number of neurons stimulated varied on a trial-by-trial basis. Neural responses can vary trial-by-trial to even identical stimulus presentations^{25–27}, rendering the flexibility endowed by two-photon optogenetics critical for tightly controlling the evoked response in the sensory stream and observing its effect on behaviour. Moreover, direct experimental stimulation of neurons is likely a critical tool for understanding activity propagation, as the activity of anatomically connected brain regions is typically highly correlated^{28,29}, but it is often unclear whether this correlated activity results from propagation between regions or from common input. Direct stimulation circumvents this issue as activity locked temporally to stimulation of a connected region likely arises from propagation. Thus, we can understand how connected brain regions coordinate by directly stimulating a given brain region, and recording a connected region, during behaviour that is causally underpinned by propagating activity.

To approach this problem, my colleagues and I imaged two hierarchically organised, densely interconnected and functionally well-characterised^{30–37} regions, the primary and secondary somatosensory cortex (S1 and S2) while performing two-photon optogenetic photostimulation of S1 neurons. We assigned behavioural salience to photostimulation by training mice through operant conditioning to report detection

of the stimulation. Photostimulation was targeted to varying groups of 5-150 neurons in S1, allowing us to parametrically adjust the effect of photostimulation, monitor its effect on behaviour and record trials spanning the perceptual threshold of the animal. By simultaneously recording neural activity occurring before and after photostimulation in both brain regions, we were able to assess how behaviourally salient stimulation is propagated through anatomically distinct brain regions.

We demonstrate that behaviourally salient photostimulation of S1 (hit trials) elicits robust activation of S2, which represents stimulus information for several seconds after stimulation. Further, we find that ongoing activity in S1 and S2, immediately preceding stimulation, influences the detectability of the upcoming stimulus. Specifically, the photostimulus detectability and propensity to propagate is greatest when both the population variance pre-stimulus in S1 is minimised and the number of cells stimulated is maximised. This is consistent with a signal-to-noise framework in which the signal is the number of photostimulated cells and the noise is the variance of the ongoing activity in S1. Thus we demonstrate that the signal-to-noise ratio of an input to a neural circuit is critical both for the behavioural salience of the input and the likelihood that the input is reliably propagated beyond the brain region in which it arises.

In this project I developed, alongside my colleagues, a novel preparation which simultaneously combined in the mouse: two-photon calcium imaging, with single cell resolution, of neural activity propagating between cortical regions and two-photon optogenetic stimulation of small groups of neurons which causally drove behaviour. To run these experiments, I built both hardware and software to run behavioural training and optogenetic stimulation in an automated manner, requiring minimal experimenter intervention during training and which automatically progressed mice through stages of training. During the final stages of training, optogenetic stimulation was delivered using holographic two-photon photostimulation, a cutting-edge optical method requiring extensive calibration and which has not previously been used in a preparation spanning multiple cortical regions. Finally, I performed

in-depth preprocessing and statistical modelling of the resulting data to draw conclusions about cortical function.

In this thesis, I introduce the methods and biological theory that underpin the project, outline how these techniques are employed in our novel preparation and explain how we employed statistical modelling to draw conclusions from the data. Finally I set these findings in the context of the field and explore how they might act to advance our understanding of cortical function.

1.1 Recording neural activity

Cortical computation is likely underpinned by populations of neurons rather than individual neurons acting in isolation^{38–40}. Hence, to understand neural coding in cortex, it is necessary to record the activity of large groups of neurons simultaneously *in vivo*. These recordings were first carried out through electrical methods in which one or more microelectrodes are inserted into the extracellular space around neurons, allowing the action potential waveform to be recorded from multiple cells^{41–43}. Recent developments to this technique has resulted in electrodes with capable of hundreds of neurons simultaneously, through thousands of channels, with exquisite temporal resolution⁴⁴. However, despite the power of this method, it has a number of drawbacks. It is often not possible to track the genetic identity or spatial relationship of recorded cells, analysis to parcel out recorded activity to individual neurons is complex⁴⁵, and stimulation of neurons during electrical recordings is limited to single-cell stimulation^{46,47} or simultaneous activation of groups of spatially co-localised neurons^{20,48–52}.

More recently, fluorescence microscopy has been applied to functional imaging *in vivo* to circumvent these issues and record large populations of neurons with single cell resolution. Generally, neural activity is recorded optically using calcium imaging⁵³, in which neurons are genetically engineered to express fluorescent molecules which undergo a conformational change when bound to calcium. As a result, the fluorescence intensity of neurons expressing these molecules increases

following calcium influx driven by an action potential⁵⁴ and spikes can be recorded optically. Currently, the most popular way to perform calcium imaging *in vivo* is through genetically encoded calcium indicators⁵⁵ such as GCaMP^{56,57}. These can be expressed in neurons long-term through viral injection⁵⁸ or in transgenic animals⁵⁹ enabling chronic imaging of the same neurons over time⁶⁰. While calcium imaging addresses the drawbacks of electrophysiology by visualising neurons, the time course of the indicator can span hundreds of milliseconds, meaning it has sub-standard temporal resolution compared to electrophysiology and resolving single-spike events can be challenging⁵⁹. Most germane to this thesis however, calcium imaging is the only method of recording neural populations that has thus far been combined with targeted two-photon photostimulation⁵⁸ (see below).

Fluorescence microscopy⁶¹ requires a light-source to excite the fluorophores in the sample. This usually takes the form of a LED or laser which bathes the entire sample simultaneously in light, allowing a sensor, such as a camera, to detect emitted photons and create an image of the sample. This is known as ‘widefield’ or ‘one-photon’ excitation. However, biological tissue is highly scattering, meaning a photon emitted from a given location on the sample may not arrive at the exact corresponding location on the sensor; additionally illumination causes the specimen to fluoresce throughout the z-dimension, resulting in photons emitted beyond the desired focal plane. Taken together these phenomena degrade the spatial resolution of the image. By contrast, scanning microscopy creates ‘optical sectioning’ by sampling regions of the sample in sequence, meaning detected photons can be assigned to a known location of the specimen⁶¹. While confocal microscopy⁶² is the most popular form of scanning microscopy it is of little use to *in vivo* mammalian neuroscience, as the wavelengths of light used to excite common fluorophores do not penetrate beyond the most superficial layers of the brain⁶³. This issue is circumvented by two-photon microscopy which, usually, employs near-infrared wavelength lasers producing photons of roughly half the energy required to excite the fluorophore in the sample. These long-wavelength lasers penetrate deep into tissue with minimal scattering and generate optical sectioning of the specimen

through multiphoton absorption. Multiphoton absorption occurs when two photons arrive simultaneously at the fluorophore and excite it by combining their energies, creating optical sectioning as the probability of this event occurring is vanishingly small beyond the focal point of the excitation beam. Hence detected photons can be confidently assigned to a small point on the sample which produces a high-resolution image up to several hundred microns deep in a sample of neural tissue⁶³.

Thus by combining calcium imaging with two-photon microscopy, the activity of hundreds of neurons can be recorded in awake behaving mice with minimal tissue lesioning^{2,64–67}.

1.2 Manipulating neural activity with light

Experiments which rely purely on recording neural activity during behaviour can be very challenging to design and interpret as it is unclear which of the sprawling array of brain regions, cell types, projection targets and neural features of interest are driving the behaviour without artificial deletion or manipulation. The current leading method in the neuroscientist's toolkit to address this is optogenetics, which combines optical and genetic technology to allow experimenters to take direct control of neurons and neural circuits. Briefly and generally, optogenetic experiments are conducted by engineering a light-sensitive protein (opsin) to a neuron, or other cell type. This allows the experimenter to shine light onto the cell and drive a current which can, for example, increase or decrease a neuron's firing rate (for reviews see^{68,69}). Optogenetics has unparalleled versatility in that experimenters can deliver loss or gain of function restricted to individual brain regions⁷⁰, genetic subtypes^{51,71,72} or projection targets⁷³ in a behaving animal⁷⁴ with tight temporal control⁷⁵.

However, in a similar vein to the issues raised above with fluorescence imaging, using widefield illumination to drive optogenetic stimulation is spatially imprecise and results in coactivation of hundreds to thousands of neurons simultaneously²¹. This likely evokes non-physiological patterns of activity, conflicting with the sparse coding

regime that has been observed in cortex⁷⁶. It is also unlikely that all stimulated neurons can be recorded. Additionally, widefield optogenetics can be targeted only to genetic subtypes of neurons and not to functionally-defined subtypes, which may drive a behaviour but be distributed throughout one or more brain regions. Finally, the same neurons are likely stimulated on each trial, meaning the effect of stimulation is challenging to vary on a trial-by-trial basis.

Recently, researchers expanded the use of two-photon technology beyond recording neurons to controlling them through optogenetics (Rickgauer, Deisseroth and Tank, 2014; Packer et al., 2015; Hernandez et al., 2016; Mardinly et al., 2018; Chettih and Harvey, 2019; Marshel et al., 2019; Daie, Svoboda and Druckmann, 2021). This greatly improves the spatial resolution of the stimulation and hence addresses the issues outlined above. The optical sectioning afforded by a two photon laser beam means that stimulation can be restricted to individual neurons. Additionally the targeted neuron(s) can be visually identified by the experimenter, meaning that, when combined with calcium imaging, functional neuronal subtypes can be identified which, for example, exhibit correlated firing with a specific behavioural event. Thus by photostimulating such neurons, their causal role in the behaviour can be assessed (Chettih and Harvey, 2019; Marshel et al., 2019; Daie, Svoboda and Druckmann, 2021).

While standard two-photon beam paths can be used to target single neurons for photostimulation, targeting multiple neurons requires more specialised optics to split the beam. The most widely used way of achieving this is through digital holography, in which a spatial light modulator (SLM) is incorporated into the beam path. Through a reflective liquid-crystal layer, this acts as a programmable two-dimensional diffraction grating, allowing arbitrary patterns to be created from the two-photon beam (Lutz et al., 2008). Thus, the researcher is able to target arbitrary combinations of neurons for optogenetic manipulation changing the identify, combination or quantity of targets on a trial-by-trial basis.

Recently, the toolkit of opsins available to researchers has expanded to include proteins particularly suited to⁷⁷ or specifically designed for^{19,78,79} two-photon optogenetic experiments. Two specific advances utilised in this thesis is the development of opsins with a red-shifted excitation spectrum, and opsins with somatic-targeting motifs. Red-shifted opsins are useful as they can be used in simultaneously with fluorescence imaging of proteins excited by blue light. Somatic-targeting improves the resolution of photostimulation, as a beam of light targeted to a cell soma is less likely to cause off-target stimulation by activating the neurites of other cells overlaying the targeted soma.

1.3 All-optical interrogation of neural circuits *in vivo*

The two-photon techniques outlined above, calcium imaging and optogenetics can be combined *in vivo* to provide a unique window into neural circuit function, enabling researchers to read and write neural activity on the level of individual neurons in behaving animals. This “all-optical” approach has yielded insight into a variety of mammalian neural systems, a non-exhaustive list of which is reviewed here. The first time all-optical interrogation was applied to *in vivo* circuit neuroscience was in the hippocampus to stimulate place cells while mice navigated in a virtual environment(Rickgauer, Deisseroth and Tank, 2014). The authors demonstrated that two-photon photostimulation could be used to mimic activity observed in its natural place field. The study also revealed that individual place cells modulate the firing of neighbouring place cells to a greater extent than previously thought, the previous model(Andersen, Bliss and Skrede, 1971) stating that “small strips of the hippocampal cortex may operate as independent functional units”. The idea of using all-optical methods to study the influence of cortical neurons on other neurons in the local circuit was subsequently employed in the visual cortex(Chettih and Harvey, 2019). Activation of excitatory neurons elicited a center-surround spatial influence profile, in which neurons close to the stimulated cell (< 70 µm) were on average excited, whereas neurons proximal but not directly neighbouring (70 - 300 µm) were

on average inhibited. Influence was balanced at distances $> 300 \mu\text{m}$. Interestingly after mapping the visual tuning of neurons, the authors found that single-neuron photostimulation was more likely to drive suppression of another neuron if the two neurons exhibited similar tuning, hinting that visual cortex may encode stimuli through feature-competition which enhances visual acuity, sparsifies the neural representation and reduces redundancy. All-optical techniques have also been used to manipulate active behaviour directly. In a technical tour-de-force in which they also developed new optics and an improved opsin specifically for all-optical experiments, Marshel et al.(Marshel et al., 2019) performed holographic two-photon photostimulation of ensembles of neurons throughout the cortical column of the primary visual cortex (V1). They showed that photostimulating co-tuned ensembles in trained mice could result in the same behavioural outcome as visual stimulation. Further, photostimulation of a subset of the neurons in an ensemble resulted in pattern completion of the remainder on the ensemble, hinting that cortical neurons exist in functional subnetworks. Finally, in anterolateral motor cortex, two-photon photostimulation of sparse subsets of neurons during behaviour elicited persistent neural activity and biased behaviour for several seconds following stimulation. This is indicative of recurrent connectivity in cortical circuits that acts to maintain inputs that are relevant to behaviour. In sum, combining two-photon calcium imaging and optogenetics has enhanced our understanding of cortical computation and its relationship to behaviour.

1.4 Somatosensory cortex as a model system

For nocturnal animals living in tunnels and burrows, somatosensation is a sense critical for survival. In rodents, the whiskers form by far the largest single somatotopic representation as these organs are crucial for navigation, threat and food detection and object localisation(Gustafson and Felbain-Keramidas, 1977). These properties make the rodent whiskers and their somatotopic cortical representation, the ‘barrel cortex’, an ideal model system for the study of mammalian sensory processing. This is because the barrel cortex is easily accessible on the cortical

surface, the sensory input is highly salient to the animal and the whiskers are easily manipulated to generate stimuli or drive an experimenter controlled behaviour. Indeed, mice have been shown to exhibit exquisite sensitivity in their ability to discriminate textures using their whiskers(Wu et al., 2013). Finally, barrel cortex activity operates in a sparse coding regime(Crochet et al., 2011) as a result, targeted optogenetic stimulation of small groups of neurons is more likely to impact behaviour than in a less sparse area.

Due to its suitability as a model system, the physiology(Feldmeyer et al., 2013) and anatomy(Petersen, 2007) of barrel cortex is well characterised and extensively studied. Generally, stimuli resulting from deflection of a whisker is represented as depolarisation throughout the barrel corresponding barrel(Crochet et al., 2011) followed by a prolonged period of inhibition(Simons, 1978) and spreading depolarisation to neighbouring barrels(Ferezou, Bolea and Petersen, 2006). The features of sensory stimulation that barrel cortical neurons are tuned to is not fully understood and is likely more complex than primary visual cortex. Neurons have been proposed to a variety of sensory events, including, but not limited to: the product of the frequency and amplitude of a whisker deflection(Arbazadeh, Petersen and Diamond, 2003), stick/slip events(Jadhav, Wolfe and Feldman, 2009), texture coarseness(Garion et al., 2014) and object location(O'Connor et al., 2010). In sum, primary sensory neurons in the somatosensory system exhibit responses spanning a variety of axes in stimulus space, making it a rich target for interrogating mammalian sensory cortical computation.

1.5 Primary and secondary somatosensory cortex

Although it is by far the most extensively studied somatosensory region, S1 does not operate in isolation, forming hierarchically organised recurrent connections with higher somatosensory regions(Felleman and Van Essen, 1991; Kamatani et al., 2007; Kwon et al., 2016). One of the major outputs of S1 is S2 (the

secondary somatosensory cortex), from which it also receives feedback connections, and activity relating to sensory processing has been shown to flow readily between these regions(Aronoff et al., 2010). Additionally communication between S1 and S2 is thought to be crucial for behaviour. These two regions have been shown to show enhanced coordination during active behaviours such as goal directed licking, with directly projecting neurons increasing their activity during behaviourally relevant touch(Chen et al., 2016). Further, S2 projecting neurons in S1 show whisking related activity not observed in primary motor cortex (M1) projecting neurons, and S2 projecting neurons encoded texture discrimination with greater fidelity than those projecting to M1(J. L. Chen et al., 2013). Finally, during a perceptual task, feed-forward neurons projecting from S1 to S2 have been shown to carry information relating to choice, with the S1-S2 loop generally encoding information related to both active touch and to behavioral choice(Kwon et al., 2016). Taken together, these results show that communication between S1 and S2 in the rodent is likely critical to paint a picture of the sensory world and guide decision making.

1.6 Propagating neural activity

As discussed above, brain areas must interact and share information to process stimuli and generate behaviour, yet how neurons shape their activity to mediate interactions is not well understood. Previous studies have studied this phenomenon by recording from multiple brain regions simultaneously during sensory stimulation and/or active behaviour. Normally, interactions are assessed by correlating activity between the two regions on a single cell or population level. Such studies have posited that: color perception may rely on communication between color responsive V1 and V2 neurons(Roe and Ts'o, 1999), attention increases coordination between visual cortical regions(Ruff and Cohen, 2016), motor preparatory activity is formatted so it is not prematurely propagated(Kaufman et al., 2014) and that activity forming interactions between brain regions exist in a communication subspace(Semedo et al., 2019). Communication between subnetworks has also been assessed in silico, which has further developed our understanding of how neural activity is

processed to facilitate propagation.. These studies have suggested that propagation is underpinned by balanced amplification, in which excitation generated by long-range recurrent connectivity is balanced by local feedback inhibition, which stabilises the network(Joglekar et al., 2018). Further, in feed-forward network models, intrinsic noise in the firing rates of neurons is critical for feed-forward propagation of inputs(Vogels and Abbott, 2005; Ozer et al., 2010). Finally the covariance structure of local population activity is thought to be critical for the propagation of activity downstream. This is because there exists a family of covariance structures that optimally propagate activity through noisy circuits; these covariances are distinct from those that represent inputs with the highest fidelity(Zylberberg et al., 2017). As the brain must both represent stimuli and propagate information it is possible that the covariance structures that exist *in vivo* may exist as a trade-off between these two phenomena, though this has not yet been assessed.

In silico studies and recordings made from multiple brain regions simultaneously have provided crucial insight into how neural activity is formatted to facilitate propagation through regions of the brain. However, causal interventions are required *in vivo* to give biological backing to in silico work and ensure that activity recorded *in vivo* is being propagated between the regions of interest, and does not result simply from common afferent input. Moreover casual manipulations can tie studies into activity propagation to behaviour by ensuring that the recorded propagating activity is behaviourally relevant.

1.7 Driving behaviour directly through cortical stimulation

The most direct way to link recorded neural activity to behaviour is by developing a behavioural paradigm dependent by definition on the recorded neurons. This is achieved by training animals to make an action based solely on experimental manipulation of activity, thus greatly simplifying the interpretation of the link between recorded activity and behavioural outcome. In primates for example,

this method has been used to establish a causal link between the probability of somatosensory cortical neurons firing and the frequency of a stimulus applied to the fingertip(Romo et al., 1998). This was achieved by training monkeys to make an action based on two frequencies of fingertip stimulation. Animals still performed the task accurately after replacing one of the stimuli with the same frequency electrical stimulation of cortical neurons in the somatotopic region corresponding to the fingertip. This ‘illusory percept’ thus demonstrates that activity in these neurons (and those activated downstream) is sufficient to guide behaviour. Surprisingly this same concept has also been applied to face recognition(Afraz, Kiani and Esteky, 2006), through a task in which monkeys were trained to distinguish face and non-face visual stimuli. This study linked face-responsive neurons in the inferior temporal cortex causally to face perception by showing that electrical stimulation of small groups of these neurons drove face detection. Thus, through causal intervention the authors unequivocally linked neurons correlative with facial stimuli to face to the active behaviour of face perception.

The idea of driving behaviour directly through electrical stimulation has also been applied in rodents. Most notably, Houweling and Brecht (2008)(Houweling and Brecht, 2008) showed that nanostimulation of single barrel cortical neurons drove behaviour to slightly above chance level, indicating that rodents are able to detect spikes in a single neuron. While this hints that the individual neurons may be more important in sensory processing than standard population coding frameworks(Averbeck, Latham and Pouget, 2006) suggest, as behavioural performance is only slightly statistically above chance, it is unlikely that single neurons underpin ethological behaviours.

Behaviour can also be driven directly through optical stimulation. This was first demonstrated by Huber et al. (2008)(Huber et al., 2008) who trained freely moving mice to lick a port to receive a reward following widefield optogenetic stimulation of S1. From this they attempted to elucidate how many neurons were required to spike in order to drive behaviour robustly (rather than to just above chance level as

in Houweling and Brecht). The authors indirectly estimated that mice could detect trains of action potentials when 60 neurons were activated simultaneously. This idea was expanded upon through the use of two-photon holographic photostimulation which has the advantage of being able to target directly a specific number of neurons, with the number varying on a trial-by-trial basis. Through this, it was shown that trains of action potentials in only 30-40 S1 neurons are required to robustly drive licking behaviour(Dalgleish et al., 2020); it is unclear whether more or less neurons are required to be stimulated in other brain regions to elicit behaviour.

Further, direct optical driving of behaviour has given insight into its computational underpinnings beyond that of the minimum number of neurons required. Through LED stimulation of S1, Histed and Maunsell (2014)(Histed and Maunsell, 2014) showed that only the total number of injected spikes, across a 100 ms window, influenced behavioural performance, the frequency or length of stimulation had no effect on performance. Hence the authors posit that animals detect stimuli by linear integration of the total number of spikes in a 100 ms window. This implies that spike timing has no impact on cortical computation and behaviour, at least in this highly non-ethological condition. However an apparently conflicting study(Gill et al., 2020) employing two-photon holographic photostimulation hints that spike counting may not be the complete picture. The authors trained mice to detect targeted activation of small groups of neurons in the olfactory bulb. They found that synchronous (less than 10 ms jitter) activation of < 30 neurons was detected more readily than asynchronous activation (≥ 30 ms jitter). This discrepancy between the two studies may be explained as first, they were conducted in different brain regions, and second two-photon holographic activation of a small number of neurons is likely much closer to the noise threshold compared to widefield activation of a large number of neurons. Hence synchronous activation may be critical if the stimulus is weak, whereas only spike counting may be required for stronger stimuli.

You might need a section on relevant neural features like E/I balance, maybe you could just pad out the bit about how neural activity is formatted

1.8 Summary

This thesis aims to stitch together the ideas presented above by applying behaviour driven directly by holographic two-photon photostimulation to the study of activity propagation between cortical regions. The barrel fields of the primary and secondary somatosensory cortex form the ideal model system for this study as they are easily optically accessible, known to be densely connected with this connectivity likely critical for behaviour, and it is known that experimental manipulation of S1 neurons can directly drive behaviour. Through this preparation I will examine *in vivo* how neural activity is formatted in S1 to enable robust propagation of activity through the cortical hierarchy, resulting in the communication between brain regions that is critical for neural processing.

2

Driving behaviour with optogenetics

Contents

2.1	One-photon photostimulation	25
2.2	Two-photon photostimulation	29

As detailed in the introduction, driving behaviour directly with experimental stimulation provides a unique window into neural computation, as recorded neurons by definition ignite the observed behaviour. This is achieved by training mice, through operant conditioning, to learn the association between artificial stimulation of neurons and reward^{17,21–24}. Two-photon holographic photostimulation is an ideal modality through which to perform stimulation as it allows for activation of a predefined number of neurons in a specific brain region which can be varied on a trial by trial basis. However, this major advantage of two-photon optogenetics is also a drawback with respect to driving behaviour, as the maximum number of neurons that can be activated simultaneously is on the order of 100. Hence, naive mice need first to be primed with more widespread activation to learn the task before the number of cells is dialed down to the number attainable by two-photon activation. This has previously been achieved by training mice to respond to

widefield "one-photon" optogenetics delivered by an LED^{23,24}.

Here, I developed a fully automated protocol for training mice to learn the association between photostimulation and reward. Mice reported detection of the stimulus by licking a spout to receive a water reward. Mice were initially trained through one-photon photostimulation with an LED. Mice learned to respond to activation of sequentially fewer neurons by reducing the LED power in a step-wise fashion when mice successfully learned to respond to a given power. Once mice had successfully learned the task at the lowest power level, in which only a few hundred neurons are likely activated²¹ they were transitioned to two-photon version of the task. Below is presented the structure of both versions of the task, as well as behavioural results.

2.1 One-photon photostimulation

Mice expressing the opsin C1V1-Kv2.1, as well as the calcium indicator GCaMP6s, were trained on the one-photon version of the task (Figure 1A), before being moved to the two-photon version. Although the two-photon stimulation light source is infrared and thus not detectable by the mouse retina, the 595 nm LED used in one-photon training is within the mammalian visual range⁸⁰. Minimal light proofing was installed in behavioural training boxes; hence it is important to rule out that mice are detecting visual cues rather than photo-stimulation. The opsin C1V1-Kv2.1 is strongly activated by 595 nm LED stimulation^{19,77}, and we compared the behavioural performance of opsin expressing mice to control mice which did not express an opsin activated by 595 nm light. Other than the virus injected, both opsin-activated and control mice were subjected to identical experimental conditions.

A fully-automated training protocol was employed to maximise repeatability; this is detailed fully in materials and methods. Briefly two trial types were delivered to the mice: go trials, in which LED stimulation was delivered, and catch trials in which no stimulation was delivered.

The stages of the automated one-photon training protocol are shown in Figure 1B. Naive mice initially learned to perform the task by pairing one-photon stimulation with reward regardless of the animal's response, referred to as the auto-reward. As the reward was not delivered before the end of the response window, the trial outcome could still be scored according to Figure 1E. Mice that scored 3 consecutive hits during the auto-reward phase were transitioned to the active phase of the task in which the trial outcome was scored in the same way, but no auto-reward was delivered. Often however, particularly during the early stages of training, mice began to fail to respond to stimulation. To refresh animals on the task, after 3 consecutive missed trials, an auto-reward was delivered on the subsequent go trial. We found a single auto-reward was enough to fully automate the training protocol and eliminate any manual intervention.

The structure of a single trial is shown in Figure 1C. To initiate a trial, mice had to withhold licking for a pseudorandomly sampled interval of 4-6 seconds. This eliminated repeated temporal structure from the task and reduced the chance of rewards by habitual licking. A 1 second response window was used to score the trial outcome. Trials were separated by a fixed 5 second inter-trial-interval. Licks during the response window were scored as hit and false positive for go and catch trials respectively, whereas withholding licking was scored as miss and correct rejection for go and catch trials respectively (Figure 1E).

We began training with high intensity stimulation (10 mW) and reduced the power as mice progressed through training (Figure 1B,D). To automate power reductions, we used the d' metric to quantify behavioural performance (see materials and methods). This metric measures the animal's detection rate while controlling for licking bias (probability of responding in catch trials). We used a conservative threshold of $d' > 2$ which mice needed to exceed before they were transitioned to the next power level.

We quantified the behavioural performance of opsin expressing mice and compared this to controls. First, we compared the number of trials required for mice to

complete the first stage of training, recording three consecutive hit trials Figure 1F. On average opsin expressing mice required fewer trials to reach this criterion (mean = X, std = X, N=14) compared to control mice (mean=X, std=X, N=4), however this difference was not significant ($p = 0.12$ Mann-Whitney U test). Next, we compared the number of trials both cohorts took to complete the task (Figure 1G,H), achieving $d' > 2$ on the lowest LED power level (0.1 mW). Opsin expressing mice required significantly fewer trials to reach this criterion (mean = X, std = X, N=14) compared to control mice (mean=X, std=X, N=4) ($p = 0.005$ Mann-Whitney U test). Finally, we compared the d' across all sessions recorded for both cohorts (Figure 1I). Sessions recorded from opsin expressing mice had a significantly higher d' (mean = X, std = X, N=X) compared to control mice (mean=X, std=X, N=X) ($p = 0.006$ Mann-Whitney U test).

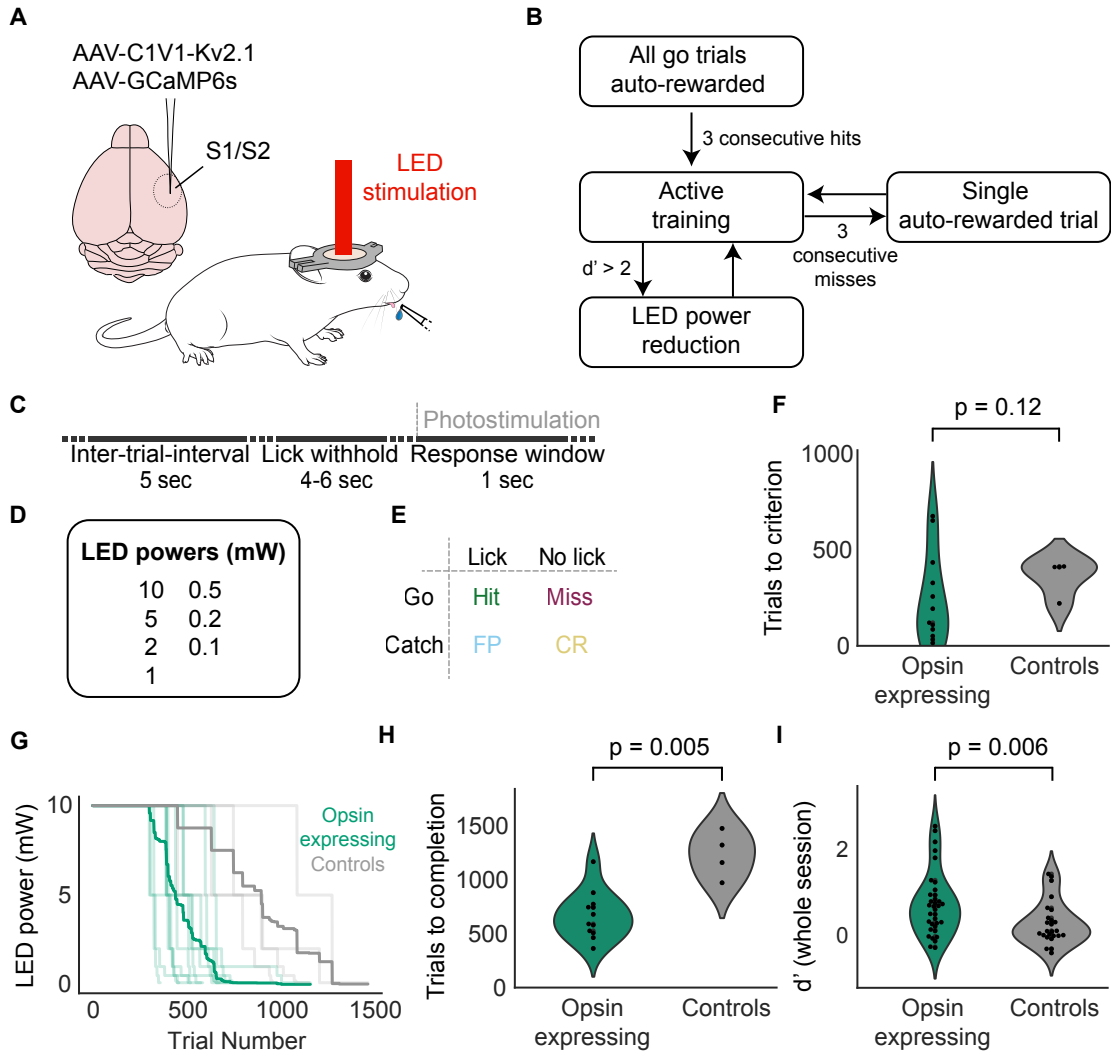


Figure 1: One-photon behavioural training. (A) Schematic of the behavioural training setup. Left: Injection into opsin expressing mice. Right: Mice were headfixed with a lick spout within reach of the tongue and photostimulation was performed with an LED. (B) Steps in the fully automated training protocol. (C) Temporal structure of a single trial. (D) LED powers used in the training. Mice started on 10 mW and were sequentially stepped down until they completed the task at 0.1 mW. (E) Behavioral response matrix showing possible trial outcomes. (F) Number of trials required for mice to reach criterion (three consecutive hit trials) and complete the first stage of the task. Each point shows an individual mouse. (G) Ladder plot showing the LED power delivered to each mouse after a given number of trials. Thin transparent lines show individual mice and thick opaque lines show the average of the cohort. Mice were removed from the average calculation once they completed the task. Mice understood the task quicker if their ladder reached lower power levels after fewer trials. (H) Number of trials to complete the task for opsin expressing and control mice. Each point is an individual mouse. (I) d' across the whole session (for all power levels). Each point is an individual session.

2.2 Two-photon photostimulation

Mice were headfixed and an objective lens was placed, immersed in water, over the cranial window. The same objective lens was used to deliver two-photon photostimulation and perform two-photon calcium imaging (Figure 2A) (See 3). The structure of the two-photon task is broadly the same as the one-photon (Figure 22D,E). However, on go trials, we directly targeted photoresponsive S1 neurons with two photon photostimulation (see 3). In addition, on catch trials, although we did not deliver photostimulating light to the brain, we moved all optical components to mimic the auditory component of go trials, meaning the animal could not perform the task from auditory queues alone. Mice were only auto-rewarded for a single trial if they recorded three consecutive miss trials. Photoresponsive S1 neurons were identified before the onset of behaviour, by photostimulating all opsin expressing neurons, in groups of 20, to find cells responsive to photostimulation.

Mice began on a version of the task with two trial types, where go and catch trials were initiated with equal probability. On all go trials, 150 S1 neurons were photostimulated (Figure 2B). Once mice achieved a $d' > 1.5$ across the entire session, they were transferred to the main version of the task, which generated the data included in all further plots.

The main version of the task introduced a third trial type, not present for initial training. Between 5 and 50 photoresponsive S1 neurons were stimulated on this trial type (Figure 2C) (see materials and methods). The behaviour of an animal on a single session is shown in Figure 2F. The lick raster indicates more reliable licking behaviour and a greater propensity to score a hit trial, when a greater number of neurons were stimulated.

The number and identity of cells stimulated was varied randomly on a trial by trial basis (see materials and methods), generating a psychometric curve (Figure 2G) which demonstrates that stimulating a greater number of neurons more robustly drove licking behaviour, and that the 50% point of the psychometric curve fit across all sessions ($N=10$) is 23 neurons (95% CI: 19–28), in accordance with

previously published findings²³. Therefore, by varying the identity and number of cells stimulated trial by trial, we delivered stimuli spanning the perceptual threshold of the animal, and ensured that the animal detects activity across the recorded population of S1 neurons rather than overtraining mice to report activity in a few specific neurons.

In sum, this chapter demonstrates that I, alongside my colleagues, was able to develop a preparation in which experimentally controlled neural activity causally drove behaviour. Progression through the stages of training were automated, maximising repeatability and minimising human intervention. As explored in the next sections, this behavioural framework means that neural activity, causally underpinning behaviour, can be recorded, with single cell resolution, both locally and after propagation downstream.

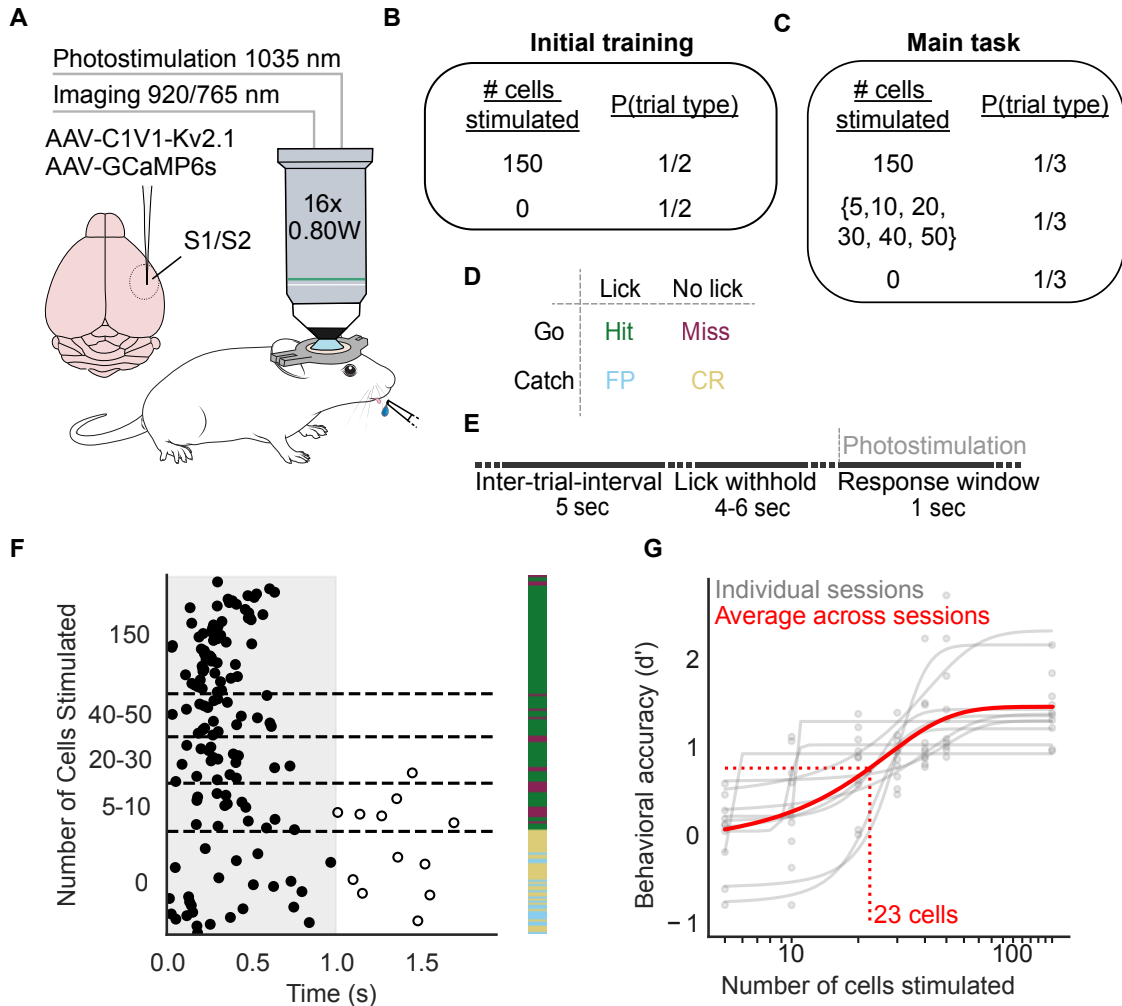


Figure 2: Two-photon behavioural training. (A) Schematic of experimental setup. *Left:* viral strategy for expression of GCaMP6s and C1V1-KV2.1-mScarlet in S1 and S2. *Right:* mice with a cranial window installed over S1 and S2 were headfixed under a two-photon microscope. A lick spout was placed within reach of the tongue, through which the animal reported perception of photostimulation by licking and received a water reward. (B) Trial types for the initial stage of two-photon photostimulation training. (C) Trial types for the main task. (D) Behavioral response matrix, colour code matches that in F. (E) Timing of a single behavioral trial. (F) Example lick raster from a single session sorted by number of cells stimulated and by time within each bin. Each row of the plot shows the first lick within an individual trial. Filled circles are licks occurring within the response window, open circles are licks occurring after the response window closes. The colourbar shows the outcome of the trial as defined in the behavioral response matrix. (G) Psychometric curves showing behavioral performance (d') as a function of the number of cells photostimulated. Each grey point is the d' computed for a given number of cells stimulated for an individual session and each grey line is a logistic function fit for an individual session. The red solid line shows the fit for all data points across all sessions ($N=10$ sessions; $N=5$ mice). The red dashed line shows the 50% point from the fit across all sessions.

3

All-optical control of neural circuits across brain regions

Contents

3.1	Localisation of S1 and S2	32
3.2	Simultaneous two-photon calcium imaging and photostimulation	34

As referenced in the previous section on behaviour, we employed an "all-optical" approach, using light to both record neural activity and experimentally manipulate it, thus driving behaviour. This approach has previously been implemented to study individual brain regions^{23,24,79,81,82}, however here we adapted previous established all-optical procedures to study multiple brain regions, and how activity propagates between them to guide behaviour.

3.1 Localisation of S1 and S2

To achieve this, we developed a preparation whereby activity in two brain regions (S1 and S2) was recorded simultaneously, while photostimulation was targeted to S1. To read and write neural activity, We expressed the genetically encoded

calcium indicator GCaMP6s⁵⁶ and the somatically targeted, red-shifted opsin C1V1-Kv2.1^{19,77} in layer 2/3 across both S1 and S2. A cranial window was implanted to enable optical access to both regions simultaneously. We localised S1 and S2 by performing wide-field calcium imaging during deflection of individual whiskers (Figure 3; methods). We stimulated whisker individually (Figure 3A), recording bulk calcium activity, and thus localising the somatotopic representation of the whisker pad indicative of S1 and S2 (Figure 3B-E). Mice were only trained on behavioural tasks if they expressed opsin in S1 and calcium indicator in S1 and S2. In subsequent all-optical experiments, a field of view was selected which spanned multiple barrels of the a, b and c row both in S1 and S2 (Figure 3B).

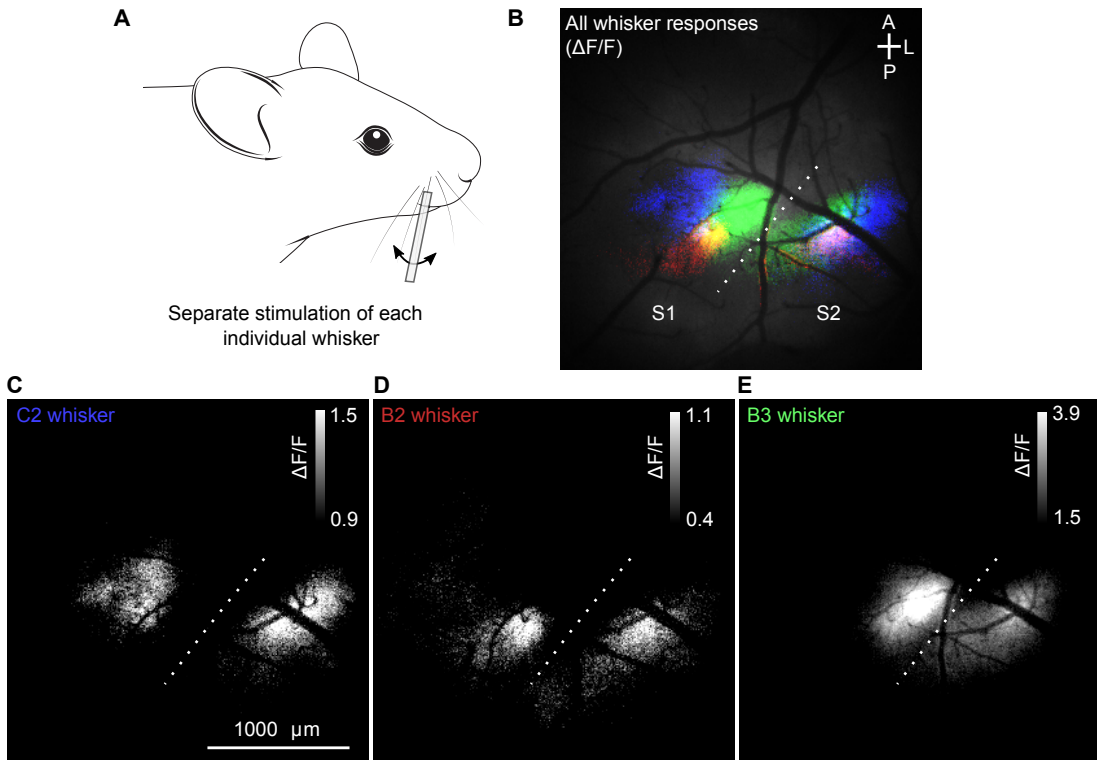


Figure 3: Widefield localisation of S1 and S2. (A) Individual whiskers of head-fixed mice were threaded into a capillary and deflected to elicit a neural response in the corresponding barrel. (B) Composite image showing a map of the barrel fields spanning S1 and S2 for an example mouse. (C) Trial averaged $\Delta F/F$ responses from bulk widefield calcium imaging, across S1 and S2, following stimulation of the C2 whisker. (D) As C but for the B2 whisker. (E) As C but for the B3 whisker.

3.2 Simultaneous two-photon calcium imaging and photostimulation

To read and write neural activity *in vivo* across brain regions in a behaving animal, we employed a two-photon microscope, based on previous designs⁵⁸, adapted to perform two-photon calcium imaging of neural activity across a large field of view (1.35 mm diameter), while performing two-photon photostimulation of S1 neurons. As outlined in the previous section, mice expressing a calcium indicator and an opsin were head-fixed and the objective lens of the microscope was placed directly over a cranial window.

Calcium imaging was performed with a resonant scanning systems (Figure 4A), scanning at 30 Hz, to excite and image the genetically encoded calcium indicator GCaMP6s³³ (Figure 2A). Spikes inferred from the slow ‘ultrasensitive’ variants of GCaMP have been shown to have correlations of >0.85 with ground truth spike trains⁸³.

To photo-activate groups of cells simultaneously, we used a microscope with a spatial light modulator (SLM) incorporated into the beam path of a laser capable of two-photon excitation (Figure 4A). The SLM contains a reflective liquid crystal layer which acts as a two-dimensional diffraction grating, and thus can be combined with holography to target multiple beamlets of light to arbitrary, user-defined points in space. This is demonstrated in Figure 4B in which fluorescence generated from 54 simultaneously generated beamlets was imaged on a wide-field camera.

The spatial resolution of an optical system is generally quantified using the point-spread function (PSF). In relation to imaging, this defines the smallest object that can be visualised, as the recorded image results from the convolution of the actual object and the PSF. The resolution of a two-photon imaging system is conventionally defined as the full width half max (FWHM) of the PSF and is usually degraded most in the axial dimension⁸⁴. The PSF can be recorded by imaging a sub-resolution fluorescence source. The axial resolution for the resonant imaging system is shown in Figure 4C left, generated by taking a "z-stack" to generate a 3-dimensional image of

the sub-resolution source from two-dimensional images taken at different focal depths. The PSF profile was then fit with a Gaussian function from the axial fluorescence intensity profile of the source, yielding a FWHM of $2.99 \mu\text{m}$. This process can be repeated with the photostimulation beam, reflected off the SLM, to generate an image of a PSF describing the profile of the photostimulation beamlet on the sample, thus quantifying the resolution of the photostimulation system (Figure 4C right, FWHM = $19.8 \mu\text{m}$). These two PSFs demonstrate that theoretically our microscope is able to read and write activity in individual neurons.

A proof-of-principle example of how the two-photon calcium imaging and optogenetics can be used to read and write neural activity is shown in Figures 4D and E. Figure 4D shows calcium activity, recorded through fluorescence imaging of GCaMP6s, a surrogate for spikes^{53,56,58,59,65}. Figure 4E demonstrates how neural activity can be injected into individual neurons expressing opsin, without driving spikes in neighbouring opsin-expressing neurons. Only the cell targeted with two-photon photostimulation exhibits a clear increase in fluorescence locked temporally to the stimulus onset.

While these proof of principle experiments prove that we can photostimulate and record from individual neurons, the behavioural experiment requires that we photostimulate groups of multiple S1 neurons, varying on a trial by trial basis, while imaging across S1 and S2. The principles behind this are outlined in figure 5. Mice expressing the calcium indicator GCaMP6s⁵⁶ and the red-shifted soma-targetted opsin C1V1-kv2.1^{19,77} were headfixed under the objective of the beam path outlined in figure 4.

A field of view was selected which spanned multiple barrels of the a, b and c row both in S1 and S2 which we could image with two-photon calcium imaging with single-cell resolution (Figure 5B,C). Before the behavioural experiment, we photostimulated all opsin-expressing neurons in multiple small groups, to find cells responsive to photostimulation, with neurons within a $350 \mu\text{m}$ diameter stimulated simultaneously. Each group of neurons was photostimulated for 250 ms, with 5 ms

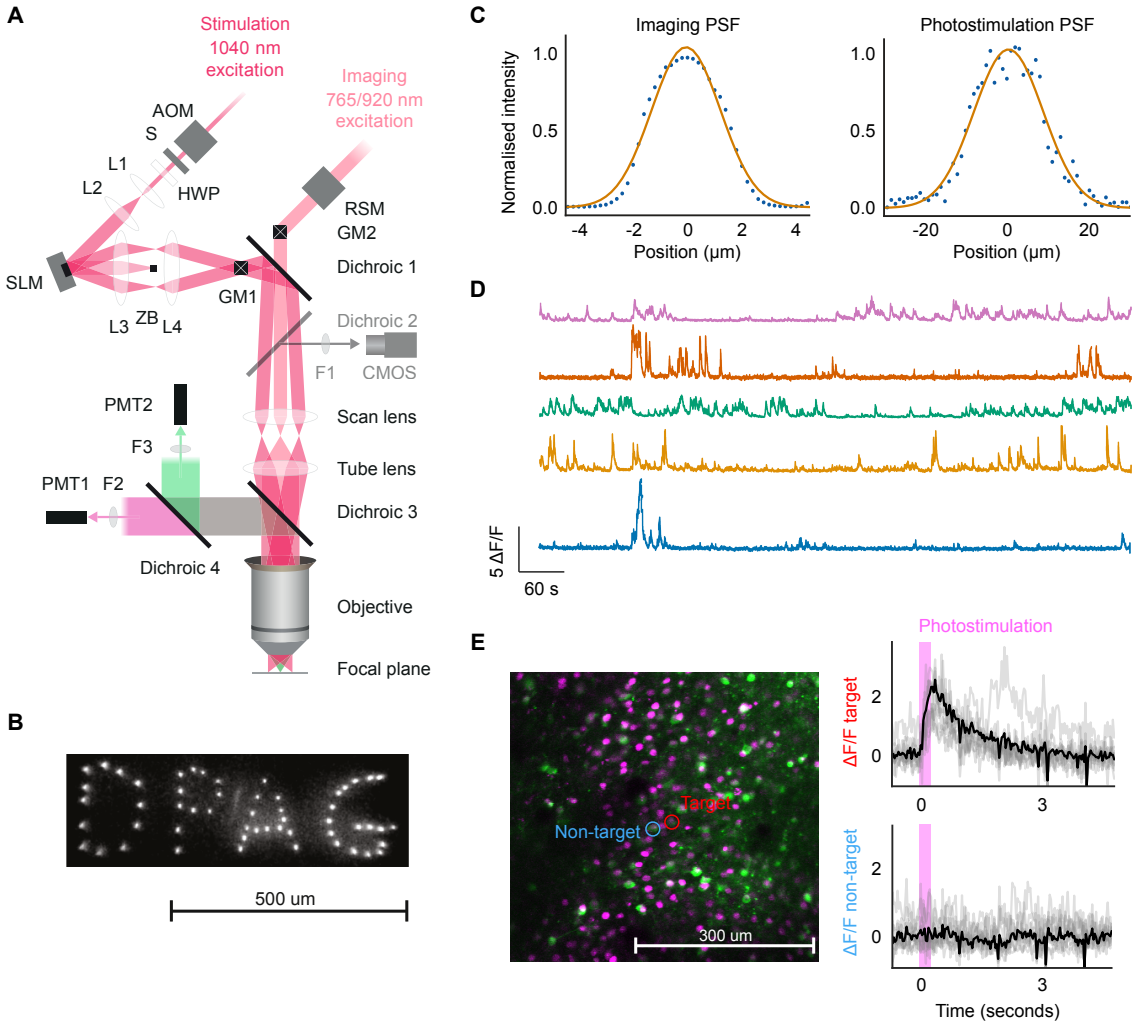


Figure 4: Two-photon calcium imaging and photostimulation. (A) Layout of the all-optical beam path. AOM, acousto-optic modulator; S, shutter; HWP, half-wave plate; L1-4, lenses; SLM, spatial light modulator; ZB, zero order block; GM1, GM2, galvanometers; RSM, resonant scanning module; F1-3, filters; PMT1, PMT2, photomultiplier tubes. Adapted from⁵⁸. (B) Beamlets generated by splitting the photostimulation beam with the SLM. For display purposes beamlets were imaged on a fluorescent plastic slide using a widefield camera (DPAG = department of physiology, anatomy and genetics). (C) Left: Axial PSF of the resonant imaging system (FWHM = 2.99 μm). Right: Axial PSF of the photo-stimulation system (FWHM = 19.8 μm). (D) Example calcium traces from 5 neurons imaged at 30 Hz. Traces were smoothed for display with a running mean of 3 frames. (E) Left: Example field of view of a mouse expressing the calcium indicator GCaMP6s (green) and the opsin ST-ChroME (magenta) (used only for this calibration experiment). The cell targeted for two-photon holographic photostimulation is highlighted in blue. Right: Fluorescence traces resulting from 10 trials of targeted photostimulation. Individual trials are shown in grey and the mean response across all trials is shown in black.

between the stimulation of each group. Trial averaged, excitatory responses to this "pre-behaviour" photostimulation can be visualised as a stimulus triggered average image (see methods) in which responses were apparent in neurons proximal to the

photostimulation beam (“targets”, defined as cells within 15 μm of the center of the beam) (Figure 4C; methods).

An demonstrative example of how multiple groups of neurons can be targeted in quick succession is shown in figure 5D. Phase masks are loaded onto the SLM, with a 5 ms inter-mask-interval, resulting in multiple beamlets of light targeted to individual cell soma. As shown in the STA images (methods) from the neural response generated by each of these masks, only cells directly under the photostimulation targets are activated by light.

As discussed in the previous section, and methods, during behavioural training we targeted between 5 and 150 photoresponsive neurons on each go trial. Groups of between 5 and 50 neurons could be targeted simultaneously with a single phase mask. The cells comprising the groups were chosen randomly with replacement on a trial by trial basis. However our system does not have the photostimulation beam power or spatial range to stimulate 150 cells simultaneously. Hence this was achieved by stimulating 3 groups of 50 neurons, resulting in a total stimulation length of 750 ms. The trial-averaged responses of targeted and non-targeted cells, both in S1 and S2, during behaviour is shown for a single session in figure 5. A clear excitatory response is only observed, when averaging across trials, in targeted neurons. As the identity of targeted cells was varied trial to trial, the cells averaged to form the traces was not the same on every trial.

In sum, this chapter demonstrates that I, alongside my colleagues, developed methodologies that allowed, all-optical techniques to be applied across multiple brain regions. This tool can then be combined with the behavioural paradigm outlined in the previous section to study neural activity, causal in behaviour as it propagates between brain regions.

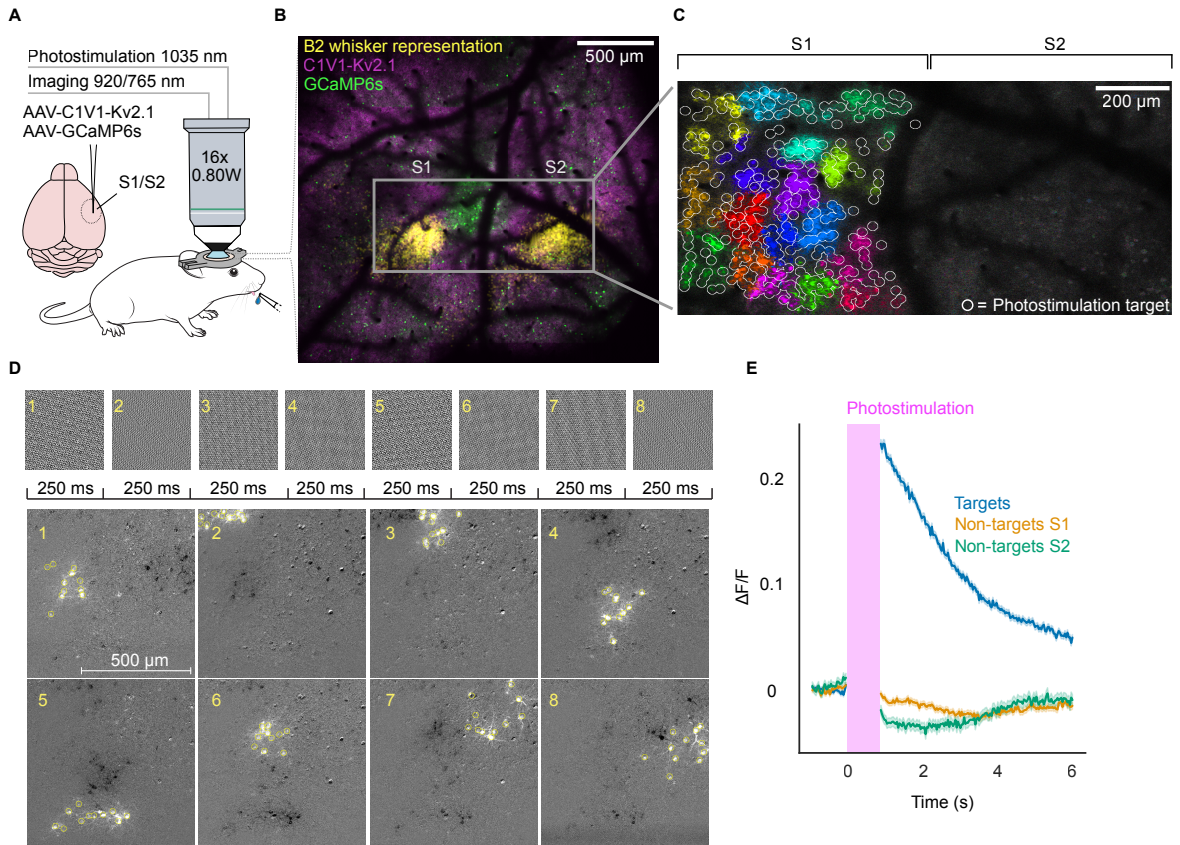


Figure 5: All-optical interrogation across brain regions **(A)** Schematic of experimental setup. Left: viral strategy for expression of GCaMP6s and C1V1-KV2.1-mScarlet in S1 and S2. Right: mice with a cranial window installed over S1 and S2 were headfixed under a two-photon microscope. A lick spout was placed within reach of the tongue, through which the animal reported perception of photostimulation by licking and received a water reward. **(B)** Example widefield calcium imaging field of view used to localise S1 and S2 by whisker stimulation. **(C)** Example two-photon calcium imaging field of view with photostimulation targets. The intensity of each pixel is proportional to the change in fluorescence intensity post-photostimulation compared to pre-photostimulation; bright pixels indicate a photostimulation-induced increase in calcium activity. Pixels are color-coded based on whether they were photostimulated simultaneously. Non-targeted cells, including those in S2 are not visible when averaging across a single stimulation group. **(D)** Sequential photostimulation. An automated protocol was used to target groups of cells for simultaneous stimulation. Groups were stimulated for 250 ms with a 5 ms inter-group-interval. 10 trials of stimulation were performed. *Top:* Phase masks loaded onto the SLM to generate targets. *Bottom:* STA images (methods). The pixel intensity of the images shows the change in $\Delta F/F$ compared to baseline, averaged across trials, in a period of 1 second immediately following photostimulation of the targets (yellow circles). **(E)** Example activity responses to photostimulation in a single behavioural session. Blue shows the response to photostimulation of cells directly targeted with light, averaged across cells and across trials. Orange and green show the response of cells not directly targeted in S1 and S2 respectively. Only trials in which photostimulation was delivered were included and data were baselined to the pre-stimulus mean on a cell-wise and trial-wise basis before averaging. Data are blanked while the photostimulation laser was on (pink bar) as this causes a large artifact unrelated to neural activity.

4

Statistical modelling of evoked neural activity

Contents

4.1	The structure of evoked activity in S1 and S2	39
4.2	Perceived photostimulation elicit persistent activity in both S1 and S2 populations	46
4.3	Pre-stimulus population in S1 predicts the upcoming trial outcome	51

To understand how neural activity is propagated between brain regions in order to guide behaviour, we used the all-optical methodology outlined in the previous two sections to compare the neural response during reported and non-reported stimuli (hit and miss trials respectively), both in the directly stimulated region (S1) and an anatomically connected downstream region (S2).

4.1 The structure of evoked activity in S1 and S2

Qualitatively, hit trials elicit a diverse array of excitatory and inhibitory responses both in S1 and S2, whereas both excitatory and inhibitory responses were less obvious on miss trials. Excited and inhibited cells are also observed in ‘reward only’

trials (methods) in which reward was delivered in the absence of photostimulation, however the population response is less pronounced compared to hit trials, indicating that the response to reported stimulation is not just explained by neural activity driven by reward (Fig. 2a; Supplementary Fig. 2,3). We find that hit trials elicit a significantly greater fraction of responsive cells in S1 compared to all other trial types, whereas in S2, hit trials elicited a significantly greater fraction of responsive cells only compared to correct rejection and reward only trials ($p < 0.05$, Bonferroni corrected). The fraction of responsive cells was greater in S2 compared to miss and false positive trials but this result was not significant ($p > 0.05$, Bonferroni corrected) (Supplementary Fig. 1,a). On a single cell level, we find individual neurons in S2 that are excited or inhibited in response to hit trials, but not miss or reward only, hinting that reported stimuli are propagated to single neurons in S2 (Fig. 2b).

Interestingly however, averaging responses across cells, trials and sessions reveals that hit trials elicit only a modest increase in population activity from baseline, immediately following stimulation, in S1 and S2, followed by a prolonged period of inhibition. Whereas the reward only condition exhibited a very different time course (Fig. 2c, Supplementary Fig. 1b,c). This hints that both brain regions exist in balanced regimes whereby excitation driven by photostimulation results in inhibition of roughly equal magnitude. Miss trials elicit excitation following photostimulation in S1, however this excitation is not observed as propagated activity in trial-and-cell-averaged responses downstream in S2 (Fig. 2c).

We next compared how the percentage of excited or inhibited neurons, both locally in S1 and downstream in S2, scaled with the number of cells photostimulated in S1 and whether this differed between perceived and non-perceived stimuli (Fig. 2d,e). As expected, stimulating more neurons in S1 excited a greater percentage of the population regardless of whether the stimulus was perceived (Fig. 2d left) (Pearson's $r = 0.62$, $p = 1.8 \times 10^{-8}$ hit trials; Pearson's $r = 0.65$, $p = 2.4 \times 10^{-9}$ miss trials). We also find that the percentage of inhibited cells in S1 also scales

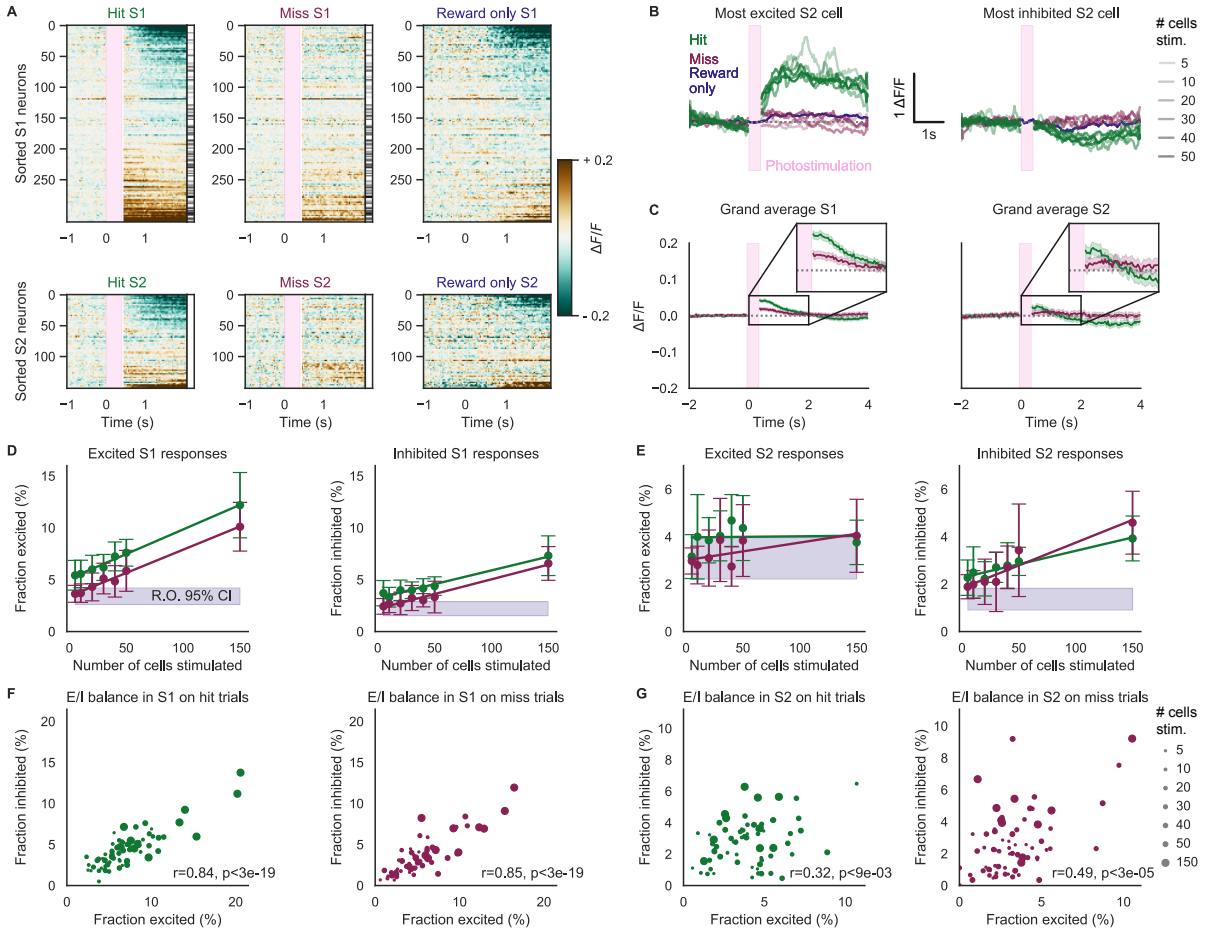


Figure 6: Structure of evoked activity in S1 and S2. (A) Raster plots showing the trial averaged response to trial types (Left: hit, Middle: miss, Right: reward only) to photostimulation (pink vertical bar, hit/miss) and/or reward (hit/reward only) of individual cells from a single session. Data were baselined to the pre-stimulus mean on a cell-wise basis before averaging. Cells are sorted by the pairwise correlation between their trial averaged responses across all three trial types (methods). A clear excitatory and inhibitory response is elicited in S1 and S2 on hit trials that cannot be solely attributed to reward. The intensity of the bar on the right hand side of the hit and miss rasters is proportional to the number of times each cell was directly targeted by the photostimulation beam. Trials in which 150 cells were stimulated were removed for display. Data are blanked while the photostimulation laser was on (pink bar). (B) Left: Example S2 cell excited on hit trials (green) but showing no response to miss trials (red) or reward only trials (blue). Each line shows an individual trial. The transparency of the line indicates the number of cells stimulated in S1. Individual trials were baselined to the pre-stimulus mean. Right: Example S2 cell inhibited on hit trials. Trials in which 150 cells were stimulated were removed for display. (C) Average population response to hit and miss trials across all sessions. Traces are averaged across cells, trials and sessions for a given trial type. Individual trials were baselined to the pre-stimulus mean. Trials in which 150 cells were stimulated were removed for display. (D) Function mapping the response in S1 on hit and miss trials to the number of cells stimulated in S1. Left: The fraction of excited cells in S1 maps linearly to the number of cells photostimulated on both hit and miss trials. Right: The fraction of inhibited cells in S1 maps linearly to the number of cells photostimulated on both hit and miss trials. The shaded purple bar shows the fraction of excited or inhibited cells in S1 on reward only (R.O.) trials. (E) Function mapping the response in S2 on hit and miss trials to the number of cells stimulated in S1. Left: There is no relationship between the fraction of excited cells in S2 and the number of cells stimulated in S1 on hit trials or miss trials. The shaded purple bar shows the fraction of excited or inhibited cells in S2 on reward only trials. Right: The fraction of inhibited cells in S2 maps linearly to the number of cells photostimulated in S1 on both hit and miss trials. (F) Population E/I balance in S1 following photostimulation. The fraction of cells excited by photostimulation in S1 is highly correlated with the fraction of cells inhibited both on hit trials (left) and miss trials (right). The size of the circle indicates the number of cells photostimulated. (G) Population E/I balance in S2 following photostimulation in S1. The fraction of cells excited by photostimulation in S1 is significantly correlated with the fraction of cells inhibited both on hit trials (left) and miss trials (right). However the magnitude of the correlation is lower than in S1. The size of the circle indicates the number of cells photostimulated.

linearly with the number of cells stimulated (Fig. 2d right) (Pearson's $r = 0.55$, $p = 1.2 \times 10^{-6}$ hit trials; Pearson's $r = 0.59$, $p = 1.4 \times 10^{-7}$ miss trials). This indicates that excitatory photostimulation elicits a compensatory inhibitory response local to the stimulation. In S2, downstream of the stimulation, however the population response to increasing numbers of stimulated cells is more complex. We find no significant relationship between the percentage of excited cells in S2 and the number of stimulated cells in S1 on hit trials or miss trials, although the correlation is an order of magnitude greater on miss trials (Pearson's $r = 0.01$, $p = 0.9$ hit trials; Pearson's $r = 0.17$, $p = 0.16$ miss trials). However we find that the percentage of inhibited cells in S2 scales linearly with the number of stimulated cells in S1 both on hit and on miss trials (Fig. 2e left, right) (Pearson's $r = 0.37$, $p = 0.002$ hit trials; Pearson's $r = 0.45$, $p = 1.2 \times 10^{-4}$ miss trials).

Next, we explicitly quantified the balance between excitation and inhibition (E/I) in both brain regions. We find robustly maintained E/I balance in S1 regardless of whether or not the stimulation was perceived, whereby the percentage of cells excited and inhibited is highly correlated (Fig. 2f) (Pearson's $r = 0.84$, $p < 3 \times 10^{-19}$ hit trials; Pearson's $r = 0.85$, $p < 3 \times 10^{-19}$ miss trials). Downstream in S2, we also find E/I balance both on hit trials and miss trials, however the correlation is less strong than in S1, and is weaker on hit trials than miss trials (Fig. 2g) (Pearson's $r = 0.32$, $p < 0.009$ hit trials; Pearson's $r = 0.49$, $p < 3 \times 10^{-5}$ miss trials). Taken together, we show that as activity is propagated away from its site of initiation, E/I balance persists but its strength is reduced. Additionally, perceived stimuli escape the balanced regime downstream to a greater extent than non-perceived stimuli as evidenced by the stronger correlation between the percentage of excited and inhibited cells on miss trials compared to hit trials.

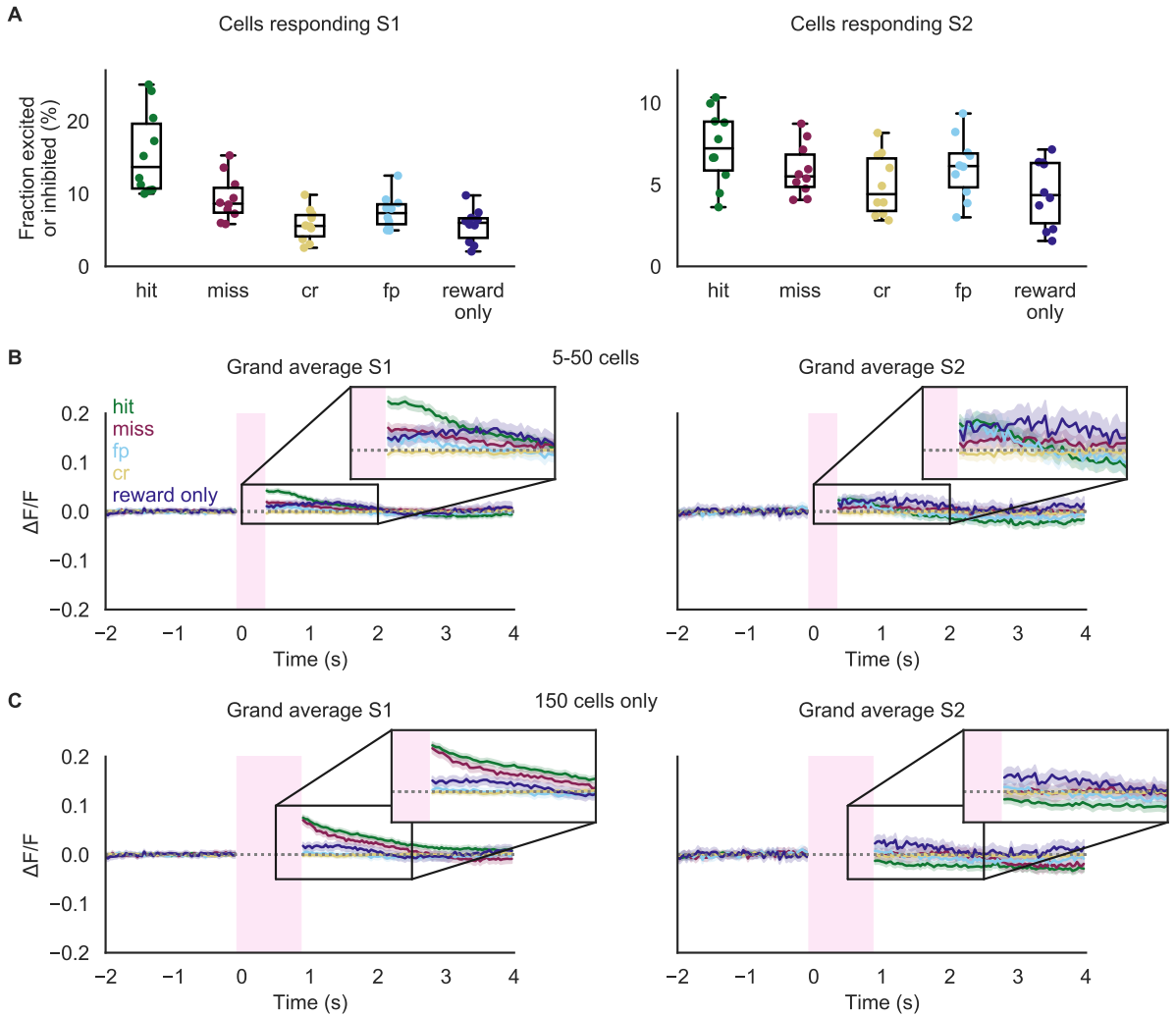


Figure 7: Fraction of cells responding and grand average traces of all trial types in S1 and S2 **(A)** The fraction of responsive cells (both excited and inhibited) on each trial type across all numbers of cells stimulated. **(B)** Average population response to all trial types across all sessions. Traces are averaged across cells, trials and sessions for a given trial type. Individual trials were baselined to the pre-stimulus mean. Trials in which 150 cells were stimulated were removed for display. **(C)** As above but including only trials in which 150 cells were stimulated.

4.1. The structure of evoked activity in S1 and S2

44

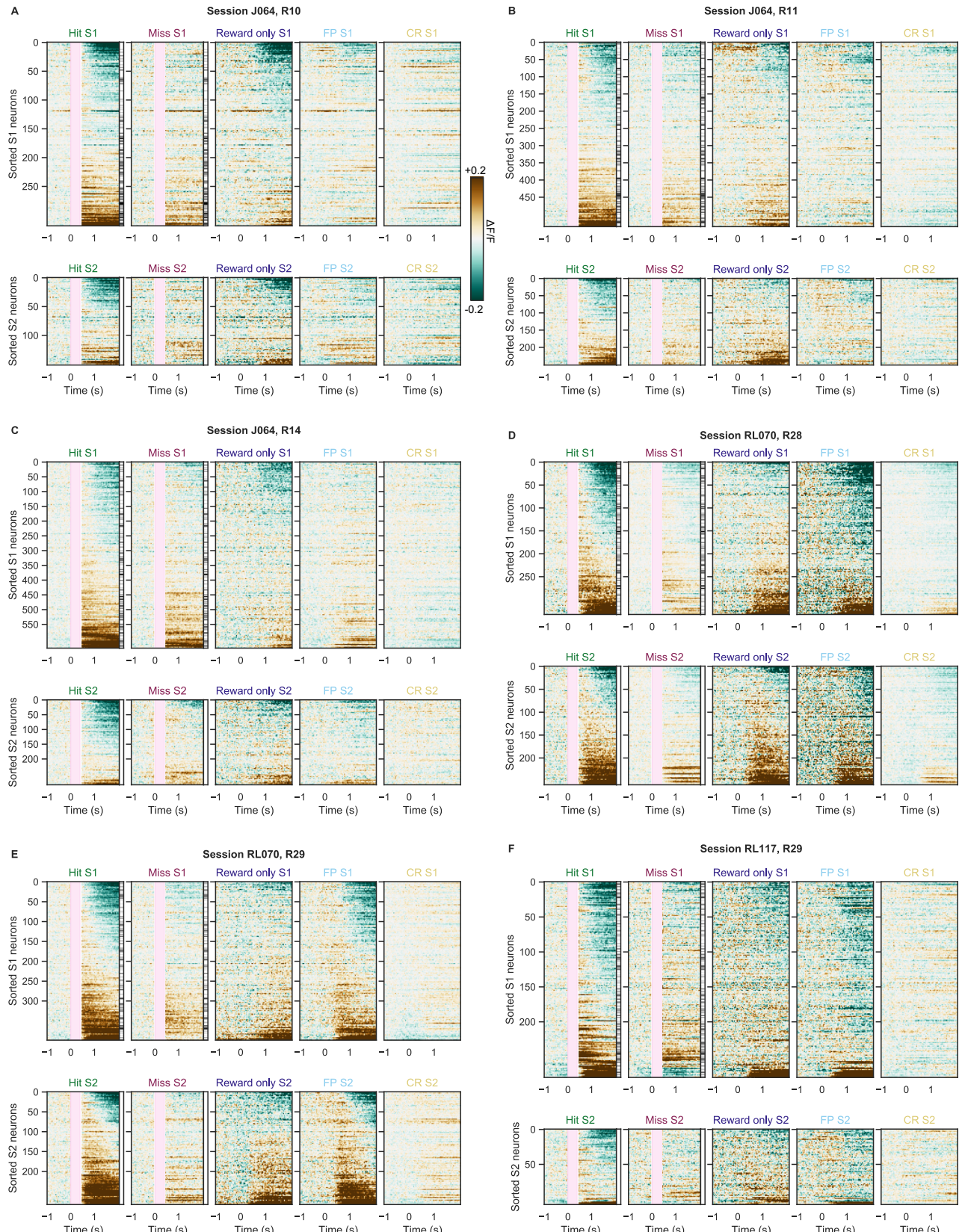


Figure 8: Trial averaged raster plots for all sessions and trial types (A-F) Raster plots showing the trial averaged response to trial types to photostimulation (pink vertical bar, hit/miss) and/or reward (hit/reward only) and/or licks (hit/reward only/false positive) of individual cells from 6 sessions. Data were baselined to the pre-stimulus mean on a cell-wise basis before averaging. Cells are sorted by the pairwise correlation between their trial averaged responses across all three trial types.

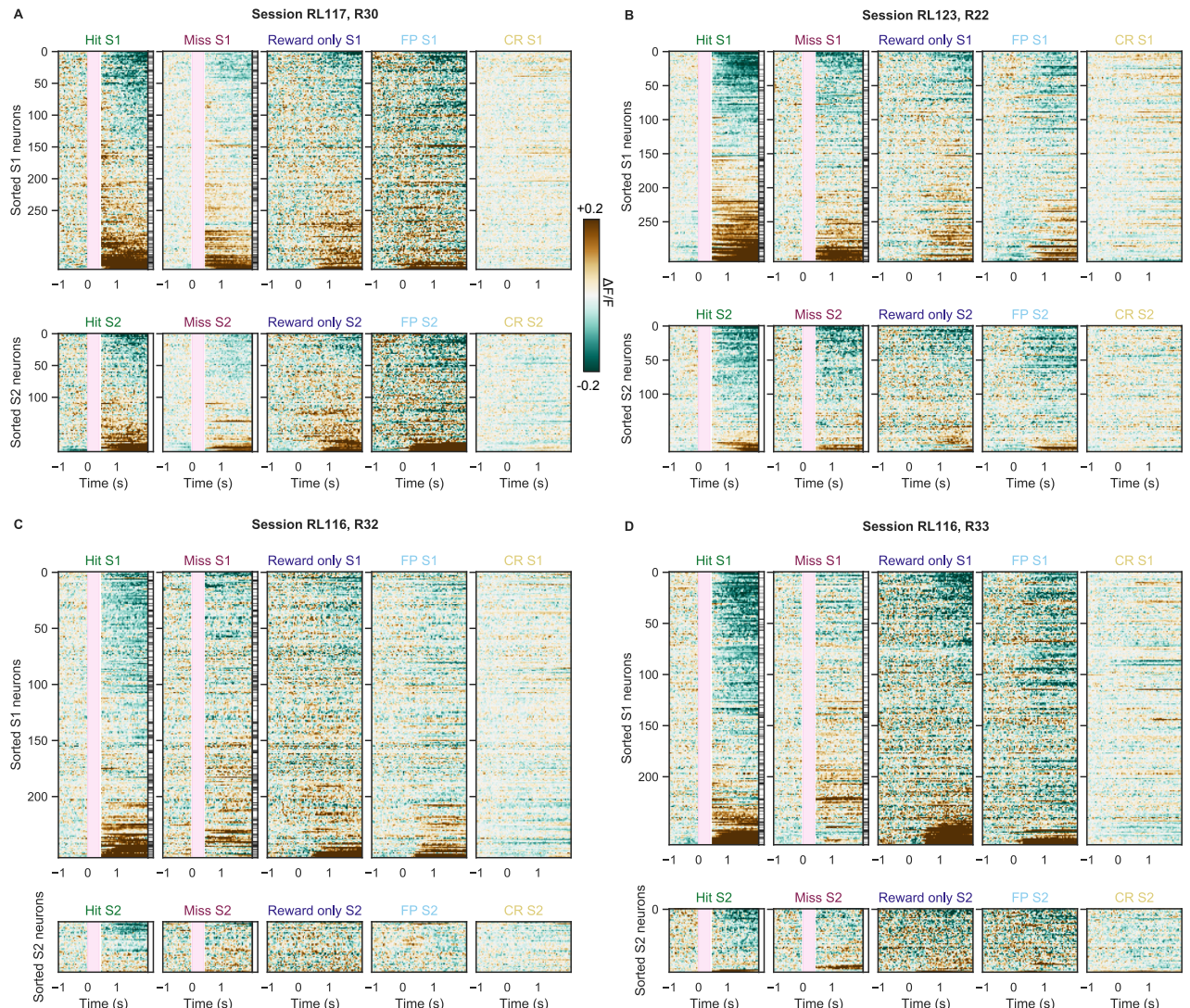


Figure 9: Trial averaged raster plots for all sessions and trial types: continued (A-D)
As above for the remaining 4 sessions

4.2 Perceived photostimulation elicit persistent activity in both S1 and S2 populations

Individual cells display a diverse array of responses, and balanced mean average responses mask the magnitude and time course of propagated activity (Fig. 2). To gain insight into these complex neural responses, we employed logistic regression classifiers on the network level and assessed propagation of stimulus-relevant activity and its relationship to behaviour. We trained classifiers to decode the trial type of individual trials using the activity of all cells in S1 or S2 on imaging data from single imaging frames. This allowed us to uncover the neural signatures of each trial type in both brain regions and quantify the temporal dynamics of this signature. First, we trained a model to classify hit trials from correct rejection trials, meaning the model should detect the neural signature of both the stimulus and the activity resulting in its perception. The classifier performed significantly above chance after stimulation and performance remained well above chance for several seconds both in S1 and S2 (two-sided Wilcoxon signed-rank test, $p < 0.05$, Bonferroni corrected) (Fig. 3a left, 3b left; Supplementary Fig. 4a,b,g,h; Supplementary Fig. 5a left, b left). Therefore, the neural activity underpinning perceived stimulation persisted both locally in S1 and downstream in S2 for several seconds. However, the classifier could be decoding the signatures of reward and the motor command required for licking, which are present on hit trials but not correct rejection trials. To address this, we tested the pre-trained classifier on reward only trials in which reward was delivered in the absence of photostimulation. In S1, performance on this trial type was either below or at chance level ($p < 0.05$, Bonferroni corrected); in S2, classifier performance on reward only trials remained at chance throughout the first 2.7 seconds of the trial (Fig. 3a left, 3b left; Supplementary Fig. 4a,b,g,h; Supplementary Fig. 5a left, b left) ($p < 0.05$, Bonferroni corrected).

As reward signals in the brain are complex, and depend on whether the reward is expected or unexpected⁴¹, we confirmed that the reward signal on hit trials and reward only trials was comparable, thus ensuring that the hit vs correct rejection

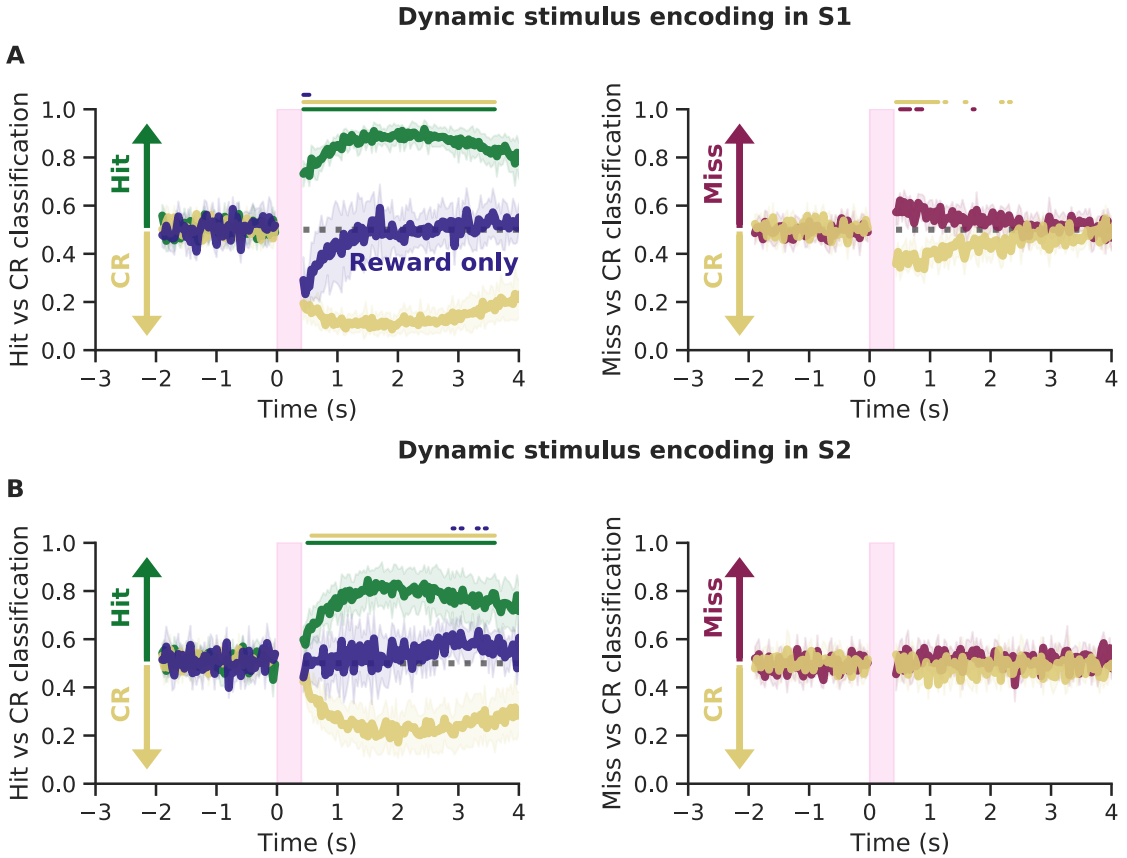


Figure 10: Perceived photostimuli elicit persistent activity in both S1 and S2 populations Dynamic decoding of trial type from neural activity in S1 using a logistic regression model. Models were trained on each frame individually, with activity from every cell in S1 or S2, and tested on held out data. Coloured bars above the traces show timepoints at which classifier performance was significantly different from chance (see methods). **(A) Left:** A model was trained on S1 activity to classify hit trials from correct rejection trials and then tested on hit trials (green), correct rejection trials (yellow) and reward only trials (blue). The model is able to classify hit trials from correct rejection trials for several seconds following photostimulation, implying that activity arising from perceived stimulation persists in S1. Reward only trials were not classified as hits, showing that the model was not just trained to decode the neural signature of reward on hit trials. **Right:** A model was trained on S1 activity to classify miss trials from correct rejection trials and then tested on miss trials (red) and correct rejection trials (yellow). The model is able to distinguish the two trial types for only for 1 second following stimulation. This implies that non-perceived stimuli do not generate persistent activity. **(B) Left:** A model was trained on S2 activity to classify hit trials from correct rejection trials and then tested on hit trials (green), correct rejection trials (yellow) and reward only trials (blue). As above, the model is able to classify hit trials from correct rejection trials for several seconds following photostimulation, implying that activity arising from perceived stimulation in S1 is propagated to S2 and persists for several seconds. Reward only trials were not classified as hits, indicating that the model was not just detecting the neural signature of reward on hit trials. **Right:** A model was trained on S2 activity to classify miss trials from correct rejection trials and then tested on miss trials (red) and correct rejection trials (yellow). The model was not able to classify miss from correct rejection trials at any timepoint, indicating that non-perceived stimuli were not robustly propagated from S1 to S2.

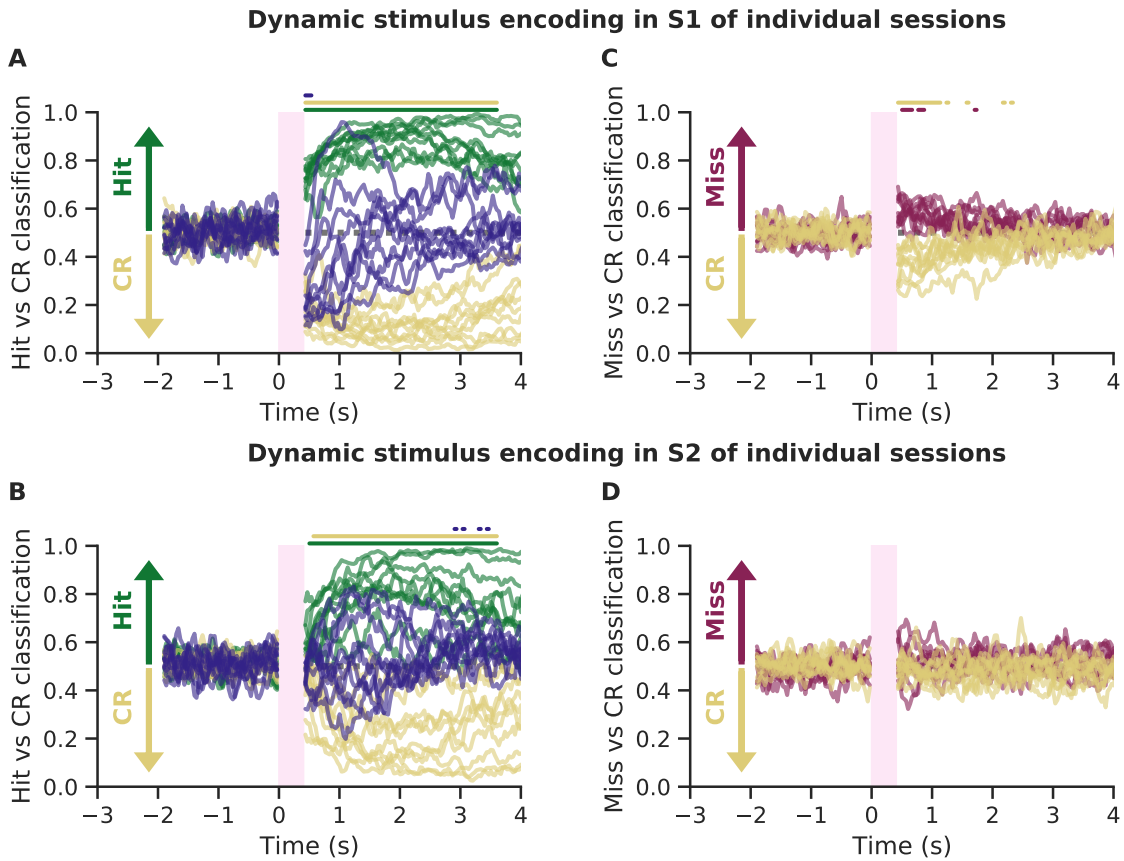


Figure 11: Dynamic decoders of individual sessions As figure 10, but displaying classifier performance for each individual sessions. Individual sessions are shown as more transparent lines, with the session average as a fully opaque line.

classifier was indeed classifying the neural signature of perceived stimulation and not just reward. This is critical as the water reward on hit trials was expected, but not expected on reward only trials. We addressed this by training a model to classify reward only trials from correct rejection trials, thus this classifier should detect only the neural signal from rewards (Supplementary Fig. 4e,f). Testing this model on hit trials resulted in identical performance to the reward only condition both in S1 and S2 (no significant difference on 110/110 time points in S1 and 108/110 time points in S2). This means that a classifier trained specifically to detect rewards could not distinguish hit and reward only trials, meaning that the neural response to reward is comparable in both trial types and the classification of hit trials from correct rejection trials is indeed decoding the neural signature of perceived stimulation, both in S1 and S2.

Next we asked whether non-perceived neural activity was reliably propagated from S1 to S2 by training a model to classify miss and correct rejection trials (Fig. 3a right, 3b right; Supplementary Fig. 4c,d; Supplementary Fig. 5a right 5b right). We found that in S1, this model decoded miss trials slightly above chance immediately following stimulation ($p < 0.05$, Bonferroni corrected), however performance rapidly decayed back to chance level after 1 second. Conversely in S2, the model did not perform above chance at any point in time, indicating that stimulus information that is not perceived does not propagate to S2.

Taken together, these results show that only perceived stimulus representations are reliably propagated out of the local brain region in which they originate to a downstream brain area. Further, stimuli that are propagated and drive perception persist both locally and downstream for several seconds following the initial injection of activity.

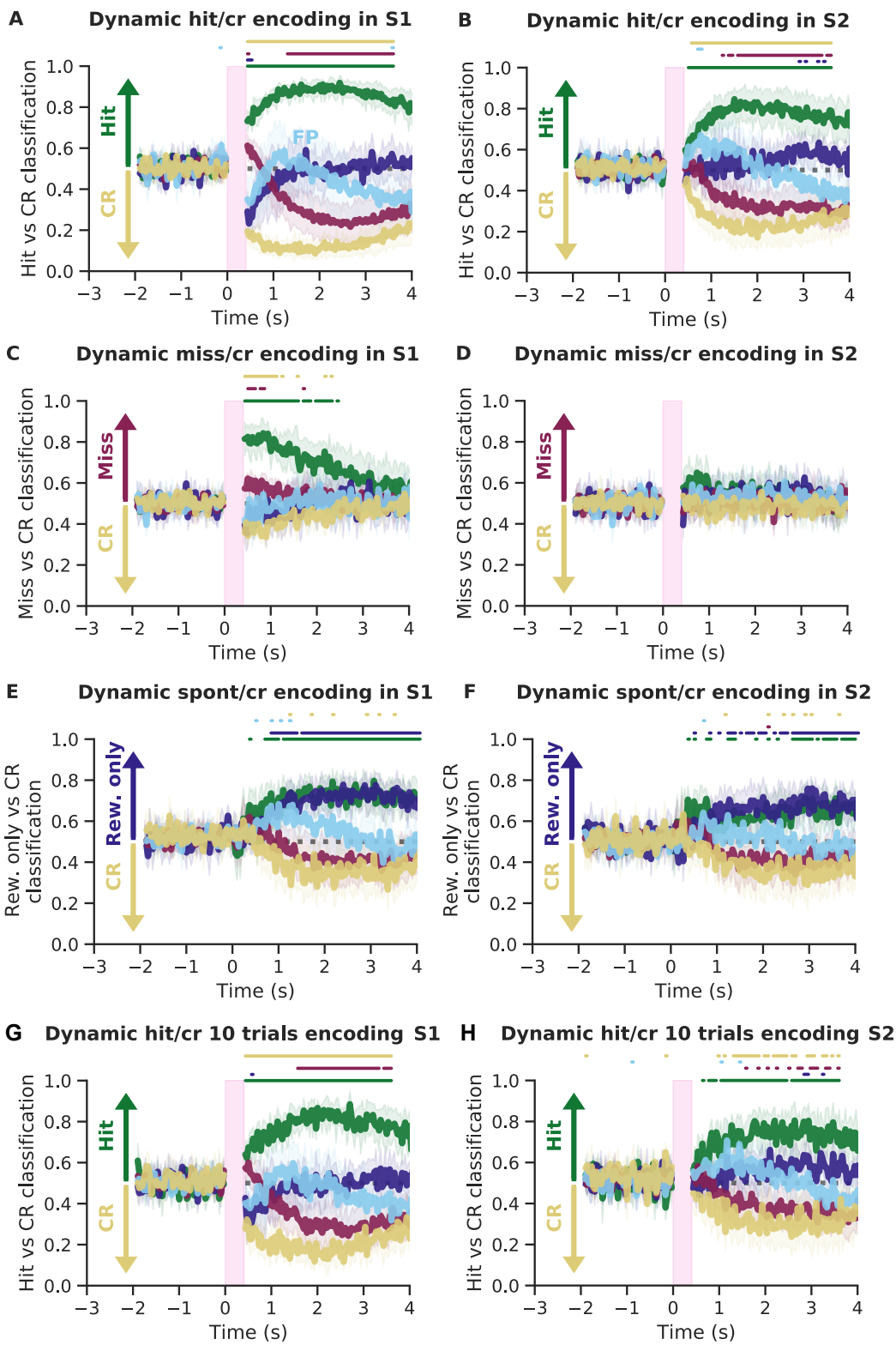


Figure 12: Dynamic decoders of all trial types

Dynamic decoding of trial type from neural activity in S1 using a logistic regression model. Models were trained on each frame individually, with activity from every cell in S1 or S2, and tested on held out data. Coloured bars above the traces show timepoints at which classifier performance was significantly different from chance (see methods). **(A)** A model was trained on S1 activity to classify hit trials from correct rejection trials and then tested on hit trials (green), correct rejection trials (yellow), reward only trials (dark blue), false positive trials (light blue) and miss trials (red). **(B)** As above, but trained on S2 activity. **(C)** A model was trained on S1 activity to classify miss trials from correct rejection trials and then tested on miss trials (red), correct rejection trials (yellow) reward only trials (dark blue), false positive trials (light blue) and hit trials (green). **(D)** As above, but trained on S2 activity. **(E)** A model was trained on S1 activity to classify reward only trials from correct rejection trials and then tested on reward only (dark blue), correct rejection trials (yellow), miss trials (red), false positive trials (light blue) and hit trials (green). **(F)** As above, but trained on S2 activity. **(G)** As **(A)** but the number of trials was restricted to 10 for each type, matching the total number of reward only trials recorded. **(H)** As **(B)** but the number of trials was restricted to 10 for each type, matching the total number of reward only trials recorded.

4.3 Pre-stimulus population in S1 predicts the upcoming trial outcome

To address the conditions facilitating both the propagation of activity to S2 and the behavioural response to stimulus, we measured population activity in S1 immediately prior to stimulation (Fig. 4a) and asked whether any statistic of the pre-stimulus population activity could predict whether the stimulus would be perceived (i.e. whether the upcoming trial type would be a hit or a miss) (see methods). This allows us to assess how population activity is formatted pre-stimulus to gate whether the upcoming stimulation propagates and thus drives perception. One basic measure of population activity is the mean, measuring whether raised or suppressed activity across S1 prior to the stimulus arriving is predictive of an upcoming hit or miss trial. We find no evidence that this metric pre-stimulus is predictive of trial type (Fig. 4.b left) (n.s.). Likewise, we find no evidence that the mean pairwise correlation between all pairs of neurons in S1 pre-stimulus increases or decreases the likelihood of stimulus detection (Fig. 4.b center) (n.s.).

One metric that clearly predicts whether the upcoming stimulus will be propagated out of S1 to drive a hit is the population variance (Fig. 4.b right), defined as the variance of the distribution of activity across S1 neurons. The lower the variance of the activity distribution pre-stimulus, the more likely the upcoming trial will be a hit. Prior to a miss trial, the variance of activity across neurons is greater than prior to a hit trial ($p < 0.002$). See Supplementary Fig. 6 for the further quantification of significant activity metrics of both S1 and S2. Additionally, population variance in S1 is correlated to population variance in S2, (Fig. 4c) (Pearson's $r = 0.53$, $p < 5 \times 10^{-85}$) demonstrating that this phenomenon is not just limited to the directly photostimulated brain region and therefore may be a metric of a more global brain state.

The relationship between population variance and behavioural performance was also evident on an individual session level, whereby population variance pre-stimulus in S1 is negatively correlated with the probability that the upcoming stimulus

elicits a hit (Fig. 4d) (one-sided regression test $p < 3 \times 10^{-12}$ on 8/10 sessions, 1 session n.s., 1 session significantly increasing). This result, taken in conjunction with Figure 1.f, shows that we have identified two separate conditions that predict the probability that the animal will successfully perceive the stimulus: the strength of the stimulus (number of cells stimulated), and the variance of the population activity (Fig. 4b,d). Next we asked if these two predictors work in tandem, where stimulus perception depends on both the strength of the stimulus and the ongoing state of the population.

We find a clear interaction in which the probability of a stimulus eliciting a hit can be expressed on a two-dimensional axis (Fig. 4e), where hit probability is highest when population variance is minimised and the number of cells stimulated is maximised. Stimulating just 5-10 neurons elicited a hit probability of greater than chance level (0.5) when pre-stimulus population variance was at its lowest level, whereas as population variance increased, more stimulated cells were required to reliably drive hits. This phenomenon can be well conceptualised in terms of a signal-to-noise ratio (SNR) framework, in which activity injected into cells through photostimulation forms the signal and the magnitude of background noise is measured as population variance. The higher the SNR, the more likely the animal is to detect the signal above ongoing noise and respond through a hit trial. Indeed, the probability of a hit is highly correlated with SNR when population variance and the number of cells stimulated are collapsed onto an SNR axis (Fig. 4f) ($p < 2 \times 10^{-10}$, logistic regression two-sided t test). Taken together, these results show that the SNR of an incoming stimulus may be critical for its continued propagation out of the local brain region where it was initiated to downstream regions where it can drive behaviour (Fig. 4g).

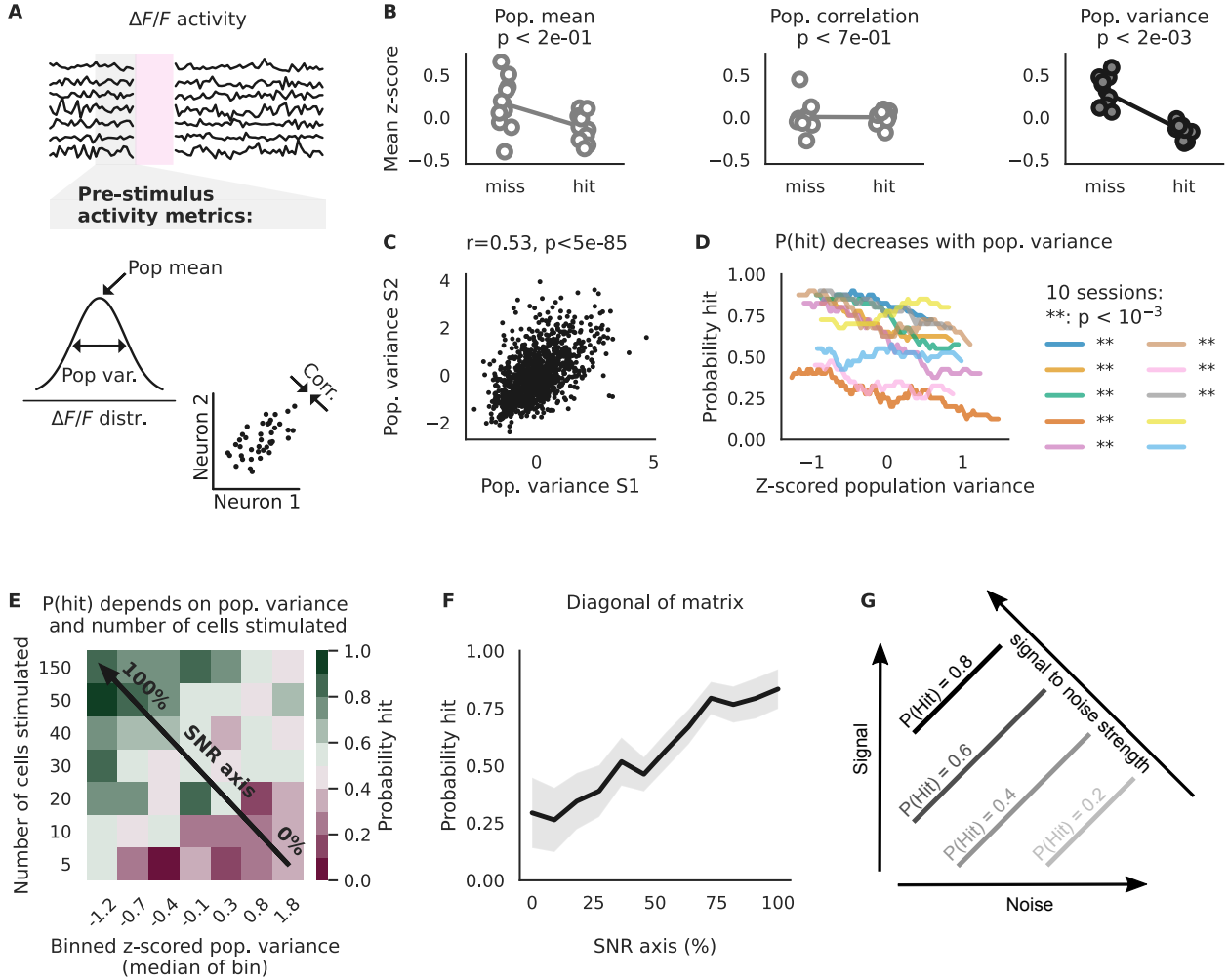


Figure 13: Pre-stimulus population in S1 predicts the upcoming trial outcome

(A) Illustration of neural activity throughout a trial. Only the activity before the stimulus on a given trial is included in subsequent plots. We considered 3 metrics of pre-stimulus neural activity; the population mean, population variance and the average absolute correlation coefficient.

(B) Comparison of population metrics of pre-stimulus S1 activity prior to hit trials and prior to miss trials. *Left:* No evidence that mean population activity pre-stimulus predicts the upcoming trial outcome. *Center:* No evidence that pre-stimulus pairwise Pearson correlation, averaged across all pairs of neurons, predicts upcoming trial outcome. *Right:* Population variance is significantly higher before miss trials than before hit trials. Pre-stimulus population metrics in S1 were computed trial-wise and z-scored across trials within a session before being split into hit and miss trials and averaged across a session. P values tested for a difference in session-wise population metrics between hit and miss trials. (C) Population variance is significantly correlated between S1 and S2 on a single-trial level. (D) The probability of a hit trial as a function of pre-stimulus population variance in S1 on a single session level. Trials within a session were binned by their z-scored population variance and this was correlated to the probability of a hit trial within that bin. 8/10 sessions show a significant negative correlation between pre-stimulus population variance and the probability of a hit. (E) The interaction between pre-stimulus population variance in S1 and the number of cells photostimulated defines the probability of a hit trial. Trials within a session were binned by their z-scored population variance and by the number of cells photostimulated; the probability of a hit within each bin was plotted on a 2-dimensional axis. This was repeated for all sessions. Maximising the number of cells stimulated and minimising the pre-stimulus variance yielded the greatest probability of a hit trial. (F) Maximising the SNR of the stimulus resulted in the maximal probability of a hit trial. Data as in f, but projected onto the ‘SNR’ axis by averaging across all bins that project orthogonally onto each point on the axis. (g) Schematic outlining the intuition for the SNR axis. Increasing the number of cells stimulated on a given trial maximises the signal of that stimulus. Noise is inversely proportional to the population variance as there is more excitation and suppression from baseline in a population with high variance. The probability of hit is maximal when SNR is maximal as the stimulus is more likely to be detected above ongoing activity.

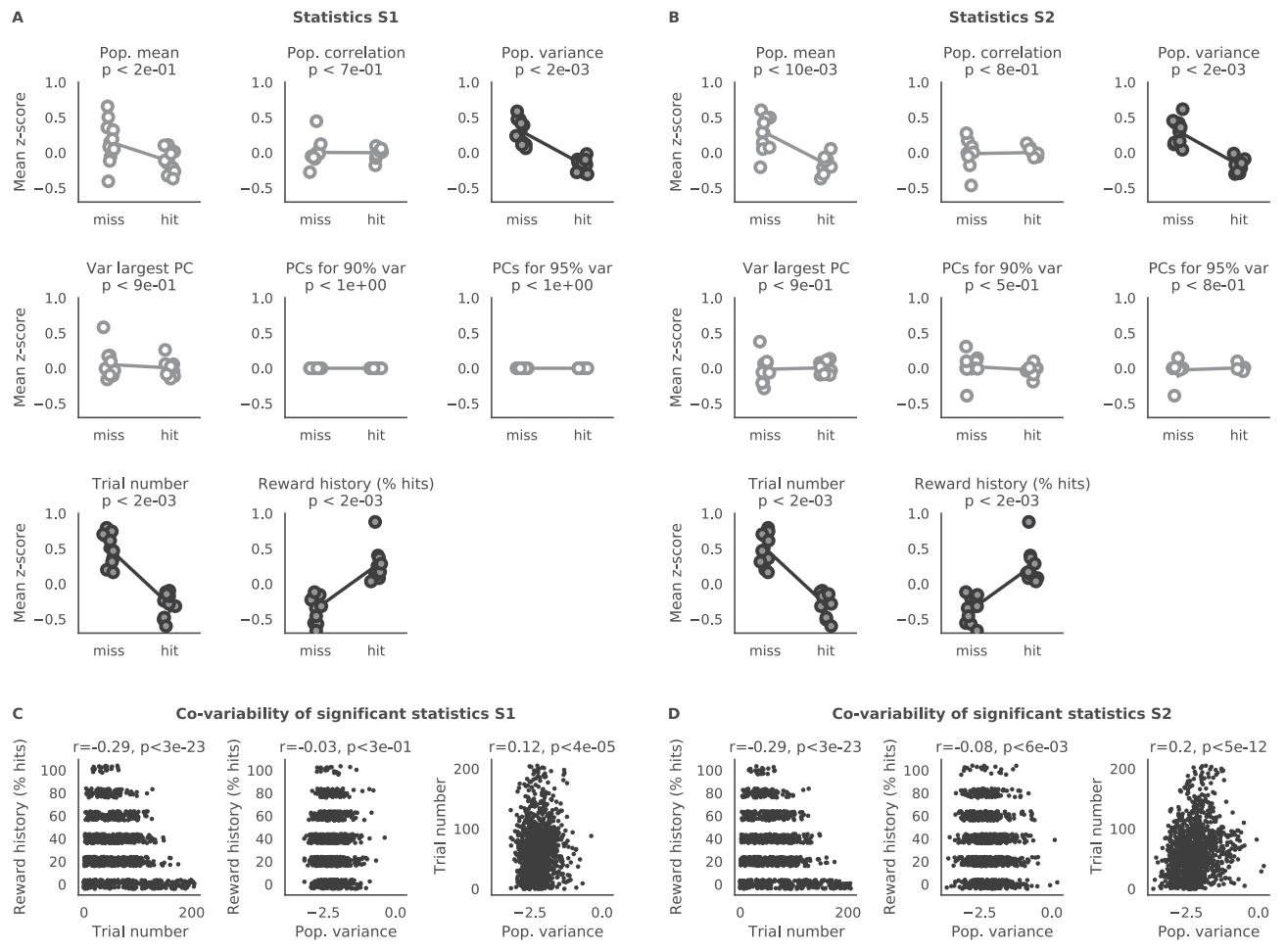


Figure 14: Further population metrics of pre-stimulus activity Comparison of population metrics of pre-stimulus in S1 (**A**) and S2 (**B**) activity prior to hit trials and prior to miss trials. The top rows show the 3 metrics of Figure 4b. The middle rows show metrics computed using Principal Component Analysis (PCA)95: the relative explained variance of the first Principal Components (PC), the number of PCs required for 90% cumulative explained variance, and the number of PCs required for 95% explained variance96. These are all metrics that indicate how well-structured, or low-dimensional, the covariance matrix is of the neural activity. These metrics are not significant which indicates that the change in population variance is not due a change in covariance structure. The bottom rows show two significant task variables; the trial number (an integer between 0 and the total number of trials in a session, indicating the number of trials previously undertaken by the animal in a given session) and the reward history (defined as % hit trials in the 5 preceding stimulated trials). (**C,D**) The co-variability of the significant statistics of panels a and b was assessed using Pearson correlation. Reward history and trial number are strongly correlated, while population variance is significant but weakly correlated to trial number in S1 and both reward history and trial number in S2.

5

Discussion

Pioneering work in systems neuroscience has greatly evolved our understanding of how the sensory world is encoded in the cortex(Hubel and Wiesel 1962; Okun et al. 2015; Stringer, Pachitariu, Steinmetz, Carandini, et al. 2019). Additionally, critical to the brain's ability to process stimuli is that activity is robustly propagated between functionally and anatomically distinct regions(Wernicke 1874; Felleman and Van Essen 1991; Zylberberg et al. 2017); however, much less is known about how neural systems coordinate to achieve this goal. While this question is often addressed in meso-scale studies of particularly the primate brain(Raichle et al. 2001; van den Heuvel and Sporns 2013), less is known about how the dynamics of neural activity are structured at the single-cell level to propagate activity between brain regions (but see(Reid 2001; Semedo et al. 2019; Vugt et al. 2018)). And as even spatially co-localised neurons can be functionally distinct(Runyan et al. 2010; Marmigère and Ernfors 2007; Kim et al. 2015; Vélez-Fort et al. 2014), single-cell resolution recordings will be necessary to understand the journey of neural activity through the brain.

We have developed a preparation with key features crucial for studying activity propagation through the cortical hierarchy. First we record simultaneously from

two hierarchically organised and densely interconnected brain regions (S1 and S2) with single cell resolution. Activity has previously been shown to readily propagate between these two regions(Pons et al. 1987; Alloway and Burton 1985; Kamatani et al. 2007; Aronoff et al. 2010) and communication between S1 and S2 has been shown to convey signals relating to active behaviour in addition to sensory stimuli(Kwon et al. 2016; J. L. Chen et al. 2016; 2013; Yamashita et al. 2013; Yamashita and Petersen 2016).

Further, in our preparation, the neural activity driving behaviour is controlled experimentally. Behaviour driven through direct cortical stimulation provides a unique window into neural function as recorded neurons unambiguously generate behavioural actions. This greatly simplifies interpretation of recorded activity as, during sensory guided behaviour, neurons in the cortex are coupled to a vast array of external variables(Stringer, Pachitariu, Steinmetz, Reddy, et al. 2019; Musall et al. 2019), as well as the internal brain state(Okun et al. 2015; Arieli et al. 1996). In addition, neural activity passes through several synapses between the periphery and the earliest sensory cortical regions, adding a layer of computational complexity at each step(McCormick and Bal 1994; Sherman 2005; King 2004). As a result, behaviour driven through direct cortical stimulation adds to our existing knowledge of cortical function, as the initiation of the neural activity underpinning behaviour can be directly recorded.

This idea has been implemented previously in mammals in a single brain region using both optical(Huber et al. 2008; Histed and Maunsell 2014; Gill et al. 2020; Dalgleish et al. 2020) and electrical stimulation(Romo et al. 1998; Houweling and Brecht 2008; Doron et al. 2014; Tanke, Borst, and Houweling 2018; Buchan and Rowland 2018), demonstrating that animals can detect activation of small groups of neurons or even single cells; these studies generally employed repeated stimulation of the same neurons trial to trial. We expand upon previous literature by employing two-photon photostimulation and varying the number and identity of stimulated cells trial by trial. As such, we ensure that mice do not become sensitive

to spikes in specific neurons and rather must tune into population events generated by co-activation of small groups of cells. This is critical as computation in the mammalian brain typically relies on populations of neurons acting in concert rather than the activity of single neurons(Averbeck, Latham, and Pouget 2006). Moreover, by performing stimulations spanning the perceptual threshold of the mouse, we were able to study population events in S1 that were detected and thus propagated to the downstream regions required to drive behaviour, such as those generating the motor command to initiate licking. We were then able to compare this to population events that were not reported by the animal. Finally, the behavioural response to two-photon activation of small groups of S1 neurons has previously been thoroughly characterised(Dalgleish et al. 2020), and we demonstrate that this behavioural paradigm is robust and reproducible as our work finds that a similar number of activated cells is required to reach the 50% point on the psychometric curve pooled across animals. Our study is different to this previous work in that we vary the identity of stimulated cells trial by trial, rather than stimulating the same groups of neurons. As we find comparable behavioural results, this implies that populations of S1 neurons are able to generalise stimuli to elicit a behavioural report, regardless of the identity of the neurons stimulated.

5.1 E/I balance

We observe a diverse array of excitatory and inhibitory neural responses to two-photon photostimulation both locally in S1 and downstream in S2. While calcium imaging with GCaMP does not visualise inhibition explicitly, it has been shown that deviations of fluorescence traces below baseline is indicative of inhibition of tonically active neurons(Vanwallegem, Constantin, and Scott 2021). We find that on average, perceived stimuli (hit trials) are represented by a short period of excitation followed by a period of inhibition. This feature is expected from recordings made in S1 during whisker stimulation(Gabernet et al. 2005; Wilent and Contreras 2005), however we show that it applies to activity arising directly from photostimulation in S1 and in activity in S2, propagated from S1. Further we show that, in agreement

with previous results(Dalgleish et al. 2020), S1 responds to excitatory two-photon photostimulation with a balancing inhibitory response. This is consistent with inhibition-stabilized networks (ISNs), formed from both strong excitatory and inhibitory recurrent connectivity. In silico, strong excitatory connectivity enables amplification of input patterns(Murphy and Miller 2009), persistent activity(Amit and Brunel 1997), and signal propagation between brain areas(Joglekar et al. 2018) while inhibition tracks excitation to prevent unstable dynamics(Sanzeni et al. 2020). We find evidence of amplification as stimulating 10s of neurons in S1 excites > 5% of recorded neurons, likely equating to hundreds or thousands of neurons total in the volume surrounding directly photostimulated cells. Next, perceived stimuli are decodable from both S1 and S2 for several seconds following photostimulation. As stimulation generally only transiently activates individual neurons, this is consistent with persistent activity resulting from recurrent connectivity(Daie, Svoboda, and Druckmann 2021; Seung 1996). This is likely not only an artifact resulting from the long temporal dynamics of calcium imaging as our persistent activity lasts longer than would be expected from the temporal dynamics of GCaMP6s(Daie, Svoboda, and Druckmann 2021; T.-W. Chen et al. 2013). Finally, we find that perceived stimuli are readily propagated from S1, and E/I balance extends to the downstream region S2 (although excitation and inhibition are less tightly coupled), consistent with data-constrained models of ISNs with long range connectivity(Joglekar et al. 2018). Taken together, we show that while populations of somatosensory cortex neurons exhibit a diverse range of responses to photostimulation of small groups of neurons, their activity is consistent with ISN models with recurrent connectivity. As perceived stimuli elicit both persistent and propagating activity, it is possible that recurrent connectivity consistent with ISN models, plays a role in this propagation.

5.2 Stimulus generalisation

We find that perceived stimuli (hit trials) are decodable from populations of neurons in S1 and S2, using a linear model. Our linear model classifies trial types in the

held-out test set, on an individual trial level, based on the weighted sum of each neuron’s activity. However the weights are trained across the entire training set, formed from multiple trials. As a result, accurate decoding of the stimulus requires that individual neurons show a consistent increase or decrease in both training set and test set trials. Although we vary the identity of stimulated neurons trial by trial, hit trials are readily decodable from S1 and S2. This means that the neural response to perceived stimulation is comparable trial to trial in both brain regions, implying that the population generalises its representation of the stimulus. On miss trials, the presence of the stimulus is only decodable for a brief period in S1 immediately following stimulation, showing that non-perceived stimuli are not generalised across both brain regions. Stimulus generalisation is a well characterised phenomenon in psychology(Pavlov 1927; Pearce 1987), biological circuits(Xu and Südhof 2013; Henschke et al. 2020) and in artificial neural networks(Sietsma and Dow 1991; Jacot, Gabriel, and Hongler 2018; Summerfield, Luyckx, and Sheahan 2020), which endows an agent with the ability to effectively interpret novel stimuli based on prior experience. This process has been shown to be enhanced if the stimulus is coupled to reward, matching our results(Henschke et al. 2020). Hence we show that generalisation of neural activity is a feature of stimuli that are both perceived and propagated between brain regions. This generalisation is also observed in a downstream region from where the activity was initiated, implying that perceived neural activity may remain generalised throughout its journey through the cortex.

5.3 Signal-to-noise ratio

The signal-to-noise ratio (SNR) of a sensory neuron(Barlow and Levick 1969) or population of neurons(Zohary, Shadlen, and Newsome 1994) is often used to quantify the fidelity of the representation of a stimulus, whereby a higher SNR means that the sensory stimulus is more robustly represented as neural activity. Indeed, one of the functions of the highly recurrent circuitry in sensory cortex is thought to be the amplification of relevant activity arising from feedforward inputs, in order

to enhance SNR(Douglas et al. 1995; Ganguli et al. 2008). Despite the well-characterised importance of high SNR in the local representation of sensory stimuli, less is known about how the SNR of a stimulus relates to its likelihood to propagate downstream. Here we replace the feedforward inputs employed in silico with direct cortical activation and quantify noise as the population variance. We find that the probability a photostimulus was perceived, and was thus propagated downstream, is dictated by the SNR of the stimulus. The relationship between noise and signal propagation has been extensively studied in artificial neural networks(Vogels and Abbott 2005; Diesmann, Gewaltig, and Aertsen 1999; Ozer et al. 2010; Guo and Li 2011). These studies show that a degree of ongoing noise is necessary for reliable propagation of activity packets between layers, however an excess of noise disrupts propagation(Guo and Li 2011). These in silico results are supported here as the cortex does not operate in a zero-noise regime *in vivo*(Vreeswijk and Sompolinsky 1998; Faisal, Selen, and Wolpert 2008; Anderson et al. 2000; Burns and Webb 1976; London et al. 2010), therefore we never observe a scenario where additional noise supports propagation. Taken together, we show that high signal-to-noise ratio activity is more reliably propagated between distinct regions of the mammalian cortex.

Although we find evidence that signal-to-noise ratio is a key neural feature facilitating activity propagation, we do not find evidence that inter-neuronal correlations are involved in this process. This appears to contrast with an elegant modelling study(Zylberberg et al. 2017) which showed that robust activity propagation between upstream and downstream cell layers was dependent on the covariance structure in the first layer. However this finding was made by varying the covariance matrix of the first later on a trial by trial basis and examining the effect on the second layer. We are not able to control the covariance matrix of an entire cell layer *in vivo*, hence further work is required to examine how the covariance structure of a population impacts its ability to propagate activity.

In sum, our study examines for the first time how injecting activity into small groups of neurons in an upstream brain region impacts both behaviour and propagation of activity to a downstream region. Through this, we find indications that the somatosensory cortex operates as an ISN, that the connectivity structure of the ISN may assist in propagating activity and that both stimulus generalisation and signal-to-noise ratio are key neural features that may participate in ensuring robust stimulus propagation to coordinate brain regions and drive behaviour.

5.4 Futher work

Further work with experimental manipulations of neural activity, such as two-photon photostimulation, is required to more closely examine how E/I balance, stimulus generalisation and signal-to-noise ratio impacts propagation of activity and its relationship to behaviour. Specifically, the causal link between these features of neural activity, behaviour and propagation could be further established using a closed-loop approach(Zhang et al. 2018) whereby neural features such as noise are monitored online(Giovannucci et al. 2017). Photostimulation could then be delivered, for example, when the stimulated population is in a low-noise state and a high-noise state. Stimuli delivered in a low-noise state should elicit more robust propagation of activity and show an increased likelihood of driving a hit trial.

It also follows from this work that feedback propagation of activity could be studied in the same framework. Most obviously, mice could be trained to report photostimulation of S2 neurons, while propagation of activity to S1 is monitored. Feedback of activity from higher to lower brain regions in the canonical pathway of sensory information flow plays a key role in many theories of cortical function(Rao and Ballard 1999; Lillicrap et al. 2020). Hence studying how feedback activity is propagated and the states employed by the brain to facilitate this could advance our understanding of cortical computation. Finally, it has been shown that mice can perceive optogenetic stimulation regardless of the brain region to which it is applied(Luis-Islas et al. 2021). Hence the preparation described here could

be applied to study any brain region, or the connections between them, and so further work could focus on whether propagating activity is shaped in the same way throughout the brain, or whether motor, frontal or subcortical regions employ a different strategy. Overall the experimental setup we describe here has great utility for assessing a wide range of brain regions, features of neural activity and theories of brain function.

If you wanna be on the bleedin' edge you gotta bleed

— Adam Packer

6

Materials and Methods

Contents

6.1	Animal usage	63
6.2	Surgical Procedures	64
6.3	Two-photon imaging	65
6.4	Widefield imaging	65
6.5	Two-photon optogenetic stimulation	66
6.6	Behavioural training	67
	One-photon behavioural training	69
	Two-photon behavioural training	70
6.7	Imaging Data analysis	71
6.8	Pre-stimulus population metrics	73
6.9	Normalisation and sorting of post-stimulus neural activity	74
6.10	Logistic regression classifiers	74
6.11	Behavioural data analysis	76
6.12	Statistical procedures	76

6.1 Animal usage

All experimental procedures involving animals were conducted in accordance with the UK animals in Scientific Procedures Act (1986).

Male and female C57/BL6 and Tg(tetO-GCaMP6s)2Niell mice were used for all experiments. Mice were between 4-12 weeks of age when surgery was performed.

6.2 Surgical Procedures

Animals were anaesthetised with isoflurane (5% for induction, 1.5% for maintenance) during all surgical procedures. A perioperative injection of 0.1 mg/kg buprenorphine (Vetgesic), 5 mg/kg meloxicam (Metacam) was administered. Mice were prepared for chronic imaging experiments through a single surgery. 2 mg/kg Bupivacaine (Marcaine) was applied to the scalp before it was sterilised with chlorhexidine gluconate and isopropyl alcohol (ChloraPrep) before being removed bilaterally. The skull was cleaned with a bone scraper (Fine Science Tools) to remove the periosteum. An aluminium head-plate with a 7 mm imaging well was bonded to the skull using dental cement (Super-Bond C&B, Sun-Medical). A 3 mm circular craniotomy was drilled over the right somatosensory cortex, targeting the S1/S2 border (-1.9 mm posterior, +3.8 mm lateral), using a dental drill (NSK UK Ltd.). The skull within the craniotomy was soaked in saline before removal. Any blood was flushed with saline for >5 minutes, before a durotomy was performed. A single 1 μ l viral injection was performed using a calibrated injection pipette bevelled to a sharp point. Injections were performed at a rate of 100 nl / minute at 300 μ m below the pial surface and were controlled using a hydraulic micromanipulator (Narishige).

The majority of mice included in this work, and all those for which behavioural training was conducted, expressed the opsin C1V1-Kv2.1. To prepare these mice, pipettes were front loaded with either: 1:10 GCaMP6s (AAV1-Syn.GCaMP6s.WPRE.SV40) diluted in C1V1-Kv2.1 (AAV9-CamKIIa-C1V1(t/t)-mScarlet-KV2.1) if injecting into C57/BL6 mice or C1V1-Kv2.1 alone if injecting into transgenic mice. Some mice, used only for calibration of the two-photon photostimulation system, were injected with 1:10 GCaMP7s (AAV1-Syn-jGCaMP7s-WPRE), 1:7 ST-ChroME(AAV9-CAG-DIO-ST-ChroME-P2A-H2B-mRuby3) and 1:7 cre (AAV1-hSyn-Cre-WPRE-hGH), diluted in sterile PBS.

After injection, a double tiered cranial window composed of a 4 mm circular coverslip glued to a 3 mm circular coverslip was pressed into the craniotomy and sealed

with cyanoacrylate (VetBond) and dental cement. Mice were recovered in a heated recovery chamber and kept under observation until behaving normally. Mice were subsequently monitored and their weight recorded for 7 days following surgery. Mice were allowed to recover for at least 21 days with ad libitum access to food and water before further procedures. This also allowed viral expression to ramp up before behavioural training was commenced.

6.3 Two-photon imaging

Two-photon imaging was performed using a resonant scanning microscope (2PPlus, Bruker Corporation) which raster scanned a femtosecond pulsed, dispersion-corrected laser beam (Vision-S, Coherent) across the sample at 30 Hz. A 16x/0.8-NA water immersion objective lens (Nikon) was used. GCaMP and mScarlet were imaged using a 920 nm and 765 nm beam respectively. Power on sample was controlled using a Pockels cell (Conoptics) and was kept at 50 mW for all experiments. A rectangular field of view (1024 x 514 pixels, 1397.4 x 701.4 μm), was used to image across two brain regions at 30 Hz. Imaging was controlled through PrairieView (Bruker Corporation).

6.4 Widefield imaging

Whisker stimulation during widefield calcium imaging was used to: target virus/tracer injections, determine the viability of a preparation for continued experimentation and find a suitable field of view for two-photon imaging encompassing S1 and S2 responses to a single whisker deflection. Using a camera, an LED and a dichroic/filter set, the whole cranial window was imaged using epifluorescence to measure calcium responses to whisker deflections. Each one of four whiskers (B1-B3 and C2; one at a time) was threaded into a capillary and deflected for 10 trials of 1 second each with 10 second inter-trial intervals. Each stimulation was 10 Hz and of 300 μm in amplitude at 500 μm from the base of the follicle. Responses to whisker stimulation were assessed using dFF stimulus triggered averages based on a baseline

of 1 second pre-stimulus. Two areas of response moved stereotypically anterior-posterior and medial-lateral according to the row and column of the whiskers stimulated, confirming whisker responses were being assessed.

6.5 Two-photon optogenetic stimulation

Two-photon optogenetic stimulation was conducted using a pulsed fixed-wavelength fibre laser at either 1030 nm (Satsuma HP2, Amplitude Systèmes) or 1035 nm (Monaco, Coherent) at a repetition rate of 2 MHz. Multiple individual neurons were targeted for stimulation simultaneously by splitting the laser beam using a reflective spatial light modulator (SLM) (7.68 x 7.68 mm active area, 512 x 512 pixels, Boulder Nonlinear Systems). The active area of the SLM was overfilled and the polarisation optimised for maximal first order diffraction efficiency using a half-wave plate. The zero order diffraction beam was blocked using a well bored into an optical flat using a dental drill (NSK UK Ltd).

Phase masks were loaded onto the SLM using the blink SDK (Medowlark Optics). Phase masks were computed by applying the Gerschberg-Saxton algorithm⁸⁵ to the xy coordinates of the target cell bodies. A weighted form of this algorithm was used to ensure uniform power distribution across all cells as the first order diffraction efficiency of the SLM is reduced with increasing distance from the zero order location. An image of the SLM was relayed onto a pair of galvanometer mirrors (Bruker Corporation) integrated into the two-photon imaging system. The galvanometer mirrors were programmed to generate spirals across cell somata by moving each beamlet simultaneously. Neurons were stimulated using 10 x 25 ms spirals of 15 µm diameter and 6 mW power.

The affine transformation required to map coordinates from SLM space to imaging space was computed through a custom-modified version of open-source software written in MATLAB (github.com/llerussell/Naparm) using the two-photon image created by burning arbitrary patterns into a fluorescent plastic slide. Phase masks and galvanometer voltages required to perform photostimulation were generated

using Naparm⁸¹. Voltages were applied to the galvanometers using PrairieView (Bruker Corporation). Custom written Python code was used to: select the cells for photostimulation, interface with Naparm to generate the files required to perform stimulation, interface with PrairieView to load voltage onto galvanometers and trigger photostimulation based on behavioural cues. A USB data acquisition card (National Instruments) running PACKIO⁸⁶, was used as a master synchroniser to record the frame clock of the imaging, onset of photostimulation and a pulse to synchronise imaging and photostimulation with behaviour.

6.6 Behavioural training

Mice were water restricted and given access to ~1 ml of water per day. Their weights were recorded and *ad libitum* access to water or wet mash was provided if the animal's weight dropped below 80% of the pre-restriction weight. For training, mice were head-fixed using their head-plate with their body supported in a 3d printed polylactic acid (PLA) tube. Mice became acclimatised to head-fixation and relaxed in the tube after the first 1-2 sessions. All behavioural training was controlled using the pyControl hardware and software⁸⁷ based around the micropython microcontroller. The pyControl framework acted as the master clock for behaviour by writing the timing of behavioural input and output events to disk and triggering trials and stimuli based on behavioural events.

Mice reported photostimulation by licking a metallic lick spout placed 5 mm from the tongue using a micromanipulator arm (Noga Engineering). The spout was electrically connected to the pyControl lickometer circuit (Open-ephys), which both recorded licking events and drove a solenoid valve (Lee Products) to deliver a ~2 μ l water reward.

The general structure of the task and individual trials was consistent at all stages of training. Each trial was separated by a fixed five second inter-trial-interval followed by a 4-6 second lick withhold period, where the length of the lick-withhold period was drawn randomly from a uniform distribution spanning these times. This

prevented mice learning temporal structure in the task and eliminated the utility of a strategy based around random high frequency licking. If the mouse licked during the lick-withhold period, the trial was restarted and a new withhold length was drawn from the uniform distribution.

Two trial types were delivered to the mice. During go trials, photostimulation was delivered and mice were rewarded if they licked to report perception of the stimulus. During catch trials, no photostimulation was delivered and mice were not rewarded if they licked the spout; no punishment was administered for licking on catch trials.

The 'response period' during which the mouse's licking response was recorded commenced immediately following the end of the lick-withhold period. This coincided with the onset of photostimulation in the case of go trials. The response period lasted for 1 second, and licks during this period alone were used to define the outcome of the trial. If the animal licked during the response period, this was scored as a 'hit'; failure to lick on a go trial was scored as a 'miss'. On catch trials, if the animal licked in the response period, the trial was scored as a 'false positive'; trials where the animal did not lick in this period were scored as a 'correct rejection'. A reward was delivered immediately after a correct lick on hit trials. This behaviour can thus be considered a detection task where catch trials are used to report the animal's baseline licking probability. Trial type was selected pseudorandomly ensuring no more than 3 consecutive trials of the same type. Mice were trained until they ignored 10 consecutive rewards or until 90 minutes had elapsed.

Behavioural performance was quantified using the d' metric⁸⁸ which quantifies the difference in response probability between hit and catch trials while controlling for baseline response rate. This allows for comparison of performance of mice with conservative licking strategies, who are less likely to lick on both go and catch trials, with mice that are more likely to lick on both trial types.

d' is defined as:

$$d' = z(\text{hit rate}) - z(\text{false alarm rate}) \quad (6.1)$$

where: z is the Z-transform function

The pyControl framework runs micropython, a lower level form of python compared to that available on a desktop computer and without any scientific packages. Hence, to perform calculation of d' online directly on the microcontroller, the Z-transforms of the hit and false alarm rates were calculated using a Padé approximant:

$$R_{4,4} = \frac{\sqrt{2\pi}(P - \frac{1}{2}) - \frac{157}{231}\sqrt{2\pi}^{3/2}(P - \frac{1}{2})^3}{1 - \frac{78}{77}\pi(P - \frac{1}{2})^2 + \frac{241\pi^2}{2310}(P - \frac{1}{2})^4} \quad (6.2)$$

where: $R_{4,4}$ is the 4th order Padé approximation of the Z-transform and P is the hit or miss rate.

One-photon behavioural training

Naive mice initially learned the association between photostimulation and reward through ‘one-photon’ widefield stimulation with a 595 nm LED (Cree). One-photon behavioural training was carried out in closed, light-proofed wooden boxes with the LED placed directly onto the cranial window using a micromanipulator arm (Noga). Current was supplied to the LED using pyControl and a custom designed analog driver board, allowing the power produced by the LED to be controlled programmatically. LED power was calibrated using a power meter (ThorLabs PM100D). A single trial’s photostimulation consisted of 5 x 20 ms pulses over a period of 200 ms. LED stimulation was delivered on go trials only.

Initially, mice learned the association between optogenetic stimulation and reward through conditioning in which the stimulus was paired with reward regardless of the animal’s response. Rewards that were delivered on miss trials are termed ‘auto-rewards’ and were delivered at the end of the response period. Mice rapidly learned to associate the optogenetic stimulus with reward and began licking before the auto-reward within 1-2 sessions. Mice were transitioned out of the auto-reward

phase and into active training when they scored three consecutive hit trials. During active training, mice were not auto-rewarded aside from for a single trial if they registered 4 consecutive misses; this functioned to motivate poorly performing mice during a session.

During the initial training phase and the first stage requiring active responses, LED power of 10 mW was used, with mice transitioned to progressively weaker LED powers once their performance was sufficiently high. Online performance was computed using running d' , computed across a window of 10 trials. Once animals had reached a running d' of 2, the LED power was reduced in a stepwise fashion until the lowest power (0.1 mw) was reached. Once animals had exceeded criterion at this power, they were considered to have completed the one-photon training paradigm.

Two-photon behavioural training

After learning the one-photon stimulation task, mice were transitioned to the two-photon version of the task, whereby mice responded to two-photon photostimulation targeted to S1 only. Initially mice were trained on a task in which 150 S1 neurons were photostimulated on every go trial in groups of 50, with an inter-group-interval of 5 ms. Once mice registered a $d' > 1.5$ across an entire session, they were transitioned to the main version of the task. This task consisted of three trial types selected pseudorandomly, with equal probability and with no more than three consecutive trials of the same type. On 1/3 of trials, 150 cells were stimulated in groups of three, on 1/3 of trials, cells were stimulated in a single group, with the number of targets stimulated drawn randomly from the set 5,10,20,30,40,50 with equal probability and with replacement, the final 1/3 of trials were catch trials in which no photostimulation was performed.

Before each session, photoresponsive cells were identified by performing two-photon photostimulation spanning opsin-expressing areas of S1. This generated the coordinates of 150 S1 neurons known to be responsive to stimulation. The subset

of neurons to be stimulated was selected randomly before each trial; cells in each simultaneously stimulated subset were no more than 350 μm apart.

Prior to active behaviour, 10 minutes of spontaneous imaging was performed without any photostimulation being delivered. During this time period 10 rewards were delivered with an inter-reward-interval of 10 seconds; this allowed us to assess the ‘reward only’ neural response in somatosensory cortex. Active behaviour followed spontaneous imaging, during which the mouse was rewarded only if it responded to a go trial. Neural activity was imaged throughout active behaviour but was stopped every 15 minutes to ensure the objective lens was completely immersed in water and to monitor animal welfare. The field of view was manually corrected for drift throughout the session by moving the objective to realign the field of view to a marker cell.

White noise was played to the animal throughout the session to mask auditory cues signifying the onset of stimulation and galvanometer mirrors were moved in an identical fashion on both go and catch trials. This ensured that the auditory cues generated were matched on both go and catch trials, and ensured that mice were responding to optical activation of S1 alone. Behavioural events were recorded through pyControl and photostimulation was controlled by custom written routines in Python and C.

6.7 Imaging Data analysis

Online analysis carried out during an experiment was conducted using STA-MovieMaker (<https://github.com/llerussell/STAMovieMaker>). These stimulus triggered average (STA) images displayed visually the change in activity of each pixel in the field of view post-stimulus relative to pre-stimulus, thus the pixel intensity of the image was proportional to the increase in activity driven by photostimulation. STA images were trial averaged in a group-wise fashion and colored, such that pixels of a given color represent the average activity driven by repeated photostimulation of

a given group of neurons. These images were used to manually define the coordinates of cells in S1 responsive to optical stimulation.

All further analysis was conducted offline. Calcium imaging movies were processed using Suite2p¹⁰³ and regions of interest (ROIs) corresponding to putative cell somata were manually selected. Suite2p also extracts a signal arising from the neuropil surrounding a cell body. To remove contamination of the signal arising from individual soma by the surrounding neuropil, we subtracted the neuropil signal from each cell body at each timepoint (t) according to the equation:

$$F(t) = F_{soma}(t) - F_{neuropil}(t) \times 0.7 \quad (6.3)$$

where:

F = neuropil subtracted fluorescence

F_{soma} = fluorescence from the cell's soma

$F_{neuropil}$ = fluorescence from the cell's surrounding neuropil

0.7 = neuropil coefficient⁵⁶

To ensure that cells with a bright baseline did not dominate the analysis, we computed $\Delta F/F$ for each cell using the equation:

$$\Delta F/F = (F - \bar{F})/\bar{F} \quad (6.4)$$

where:

\bar{F} = The mean of F across time through the entire session

Cells with very high $\Delta F/F$ values ($\max(\Delta F/F) > 10$) were discarded from further analysis.

Imaging data was split into individual trials, defined as 2 seconds preceding and 8 seconds proceeding the onset of a trial. Frames occurring while the photostimulation laser was on were excluded due to artifactual crosstalk in the imaging channel. Trial

onset was defined either as the onset of photostimulation in the case of go trials, the onset of galvo spiralling in the case of catch trials or the delivery of reward in the case of reward only trials.

Neurons were defined as ‘targeted’ on an individual trial if any part of their cell body was located within 15 μm of the centre of the photostimulus beamlet. Neurons were categorised as responsive or unresponsive to stimulus or reward in a trial-wise manner. For each trial, the distribution of $\Delta F/F$ values 500 ms pre-stimulus were compared to 500 ms post-stimulus for each cell. A cell was deemed as responsive to a stimulus on an individual trial if it passed a significance threshold of $p = 0.05$, using a two-sided Wilcoxon signed-rank test, following false discovery rate (FDR) correction. The alpha of the FDR correction (0.015) was set empirically as the value which yielded 5% of cells responding on correct rejection trials, where there was no stimulation or licking response. Following significance testing, cells were split into positive and negative responders based on whether the mean $\Delta F/F$ value post-stimulus was greater or less than the mean $\Delta F/F$ value pre-stimulus respectively.

6.8 Pre-stimulus population metrics

All pre-stimulus population metrics were computed across a 500 ms period immediately prior to photostimulation. All metrics were calculated on a trial-wise basis. The natural logarithm was taken of metrics that were fit better by a log-normal distribution as opposed to a normal distribution as assessed by Kullback-Leibler divergence.

Mean population activity was computed by first averaging $\Delta F/F$ activity across all pre-stimulus frames for each neuron to yield a vector containing a scalar value for each neuron defining its pre-stimulus activity. Next firing rates were averaged across all neurons to give a single scalar value for each trial, defining the average population activity.

Population variance was computed in a similar fashion, first by averaging across all pre-stimulus frames for each neuron. However rather than taking the mean of the activity vector as above, the variance of the vector was used to generate a single scalar value for each trial.

Mean pairwise correlation was computed by calculating the cross-correlation matrix for all pairs of neurons, whereby element i,j in this matrix was the Pearson correlation between neuron i and neuron j across all pre-stimulus frames. A single scalar value was generated for each trial by taking the absolute value of each element in the matrix, then computing the mean across all off-diagonal elements of this matrix.

6.9 Normalisation and sorting of post-stimulus neural activity

Post-stimulus neural activity was baselined relative to pre-stimulus activity in order to assess the relative change in activity after the photostimulation period, and to compare this change across cells and trials. On each trial, for each individual cell, the average $\Delta F/F$ activity in the 2 seconds preceding the photostimulation was subtracted from the post-stimulus activity trace. Neurons were sorted for visual clarity only (in Fig. HELLO FIX ME), using the sum of the post-stimulus $\Delta F/F$ activity on hit, miss and reward only trials. This yields a sorting from strongly inhibited to strongly excited cells.

6.10 Logistic regression classifiers

The dynamic decoding classifiers of Figure 3 used a logistic regression model with an L2 penalty term to the weights with a regularisation strength of 1. The Scikit-learn implementation of logistic regression was used⁸⁹. Classification accuracy was computed on a session-wise basis and then averaged across sessions, with error bars showing the 95% confidence interval of performance across sessions. Trials of the majority trial type class were randomly subsampled to adjust for sessions in which there was an unequal number of different trial types and ensure that models were

not biased to a major or minor class. (This meant that the reward only / correct rejection classifier could only use 10 trials: the number of reward only trials. To ensure that this low number of trials did not underlie the difference in performance with the hit / correct rejection classifier, we also trained a hit / correct rejection decoder using 10 trials only (Supplementary figure FIX ME 4g, h, hit predictions are significantly greater than reward only predictions on 94/110 post-stimulus time points in S1 and 46/110 post-stimulus time points in S2). Each model was trained to classify the probability that a trial belonged to one of two different trial types. A 3:1 train:test split was employed and model performance was assessed on held out test trials only. 4-fold cross validation was used on each session, with a new model trained for each fold, and classification accuracy is reported as the average of the test data across folds, meaning all trials were in the the held-out test set for one single fold. A new model was trained from scratch for each imaging frame within a trial, hence the training data consisted of a vector containing a single scalar $\Delta F/F$ value for each cell of all trials on a given frame.

Significance of decoding predictions was assessed by two-sided Wilcoxon signed-rank tests, where the predicted classification was compared to chance level (= 0.5). Predictions were binned per 2 time points, such that each test consisted of 20 (2 time points x 10 sessions) paired samples (prediction and the constant chance level). Predictions were said to be significant if their p value was below 0.05, Bonferroni corrected for the number of tests performed per trial type (167, both the pre-stimulus and post-stimulus activity excluding the photostimulation artifact). The binning of 2 time points was used because single time point statistics had too little data to be significant given the strong Bonferroni correction. Hence we chose the smallest bin size through which it was mathematically possible to yield significant p values. Significant time points are indicated in Fig. HELLO 3 and Supplementary Fig. 4,5 by thick lines, coloured by the trial type they refer to, at the top of each panel. To quantify the difference between predictions of two trial types, the same tests were performed comparing the two trial type predictions directly.

6.11 Behavioural data analysis

As imaging was stopped intermittently, neural activity was not recorded for every trial performed by the animal; trials that were not imaged were excluded from all analysis. Hit trials in which the animal licked with an exceptionally short-latency (<250 ms) are likely to have been driven by random licking rather than perception of the stimulus and were thus marked as 'too-soon' and not included in further analysis. The threshold of 250 ms was selected by inspecting the lick distribution on hit trials, in which lick frequency increased above baseline rate after 250 ms.

Psychometric curves were fit to behavioural data by computing the value of d' separately for trials in which a given number of cells was stimulated. This was achieved by comparing the hit rate for a given number of cells stimulated to the false positive rate across all catch trials. Data was fit using a logistic function adjusted to fit both negative and positive values. Sessions were discarded if behaviour was not well described by a psychometric function, whereby behavioural performance improved with a greater number of neurons photostimulated. Sessions were also discarded if behavioural performance was poor, where d' for trials on which 150 cells were stimulated was less than 0.95 and/or d' for trials on which 40 and 50 cells were stimulated was less than 0.5.

6.12 Statistical procedures

We did not use statistical methods to determine sample size and no randomisation or blinding was used. Unless otherwise stated, paired non-parametric tests were employed and a p value of 0.05 was used as a threshold for significance throughout. Multiple comparisons corrections were applied using the Bonferroni correction unless otherwise stated. Error bars show 95% confidence interval unless otherwise stated.

1. Mante, V., Sussillo, D., Shenoy, K. V. & Newsome, W. T. Context-dependent computation by recurrent dynamics in prefrontal cortex. *Nature* **503**, 78–84 (2013).
2. Stringer, C., Pachitariu, M., Steinmetz, N., Reddy, C. B., Carandini, M. & Harris, K. D. Spontaneous behaviors drive multidimensional, brainwide activity. *Science* **364** (2019).
3. Hubel, D. H. & Wiesel, T. N. Receptive fields, binocular interaction and functional architecture in the cat's visual cortex. *The Journal of Physiology* **160**, 106–154 (1962).
4. Simons, D. J. Response properties of vibrissa units in rat SI somatosensory neocortex. *Journal of Neurophysiology* **41**, 798–820 (1978).
5. Carandini, M., Heeger, D. J. & Movshon, J. A. Linearity and Normalization in Simple Cells of the Macaque Primary Visual Cortex. *Journal of Neuroscience* **17**, 8621–8644 (1997).
6. Okun, M., Steinmetz, N. A., Cossell, L., Iacaruso, M. F., Ko, H., Barthó, P., Moore, T., Hofer, S. B., Mrsic-Flogel, T. D., Carandini, M. & Harris, K. D. Diverse coupling of neurons to populations in sensory cortex. *Nature* **521**, 511–515 (2015).
7. Stringer, C., Pachitariu, M., Steinmetz, N., Carandini, M. & Harris, K. D. High-dimensional geometry of population responses in visual cortex. *Nature* **571**, 361–365 (2019).
8. Britten, K. H., Shadlen, M. N., Newsome, W. T. & Movshon, J. A. The analysis of visual motion: a comparison of neuronal and psychophysical performance. *The Journal of Neuroscience* **12**, 4745–4765 (1992).
9. Platt, M. L. & Glimcher, P. W. Neural correlates of decision variables in parietal cortex. *Nature* **400**, 233–238 (1999).
10. Yang, T. & Shadlen, M. N. Probabilistic reasoning by neurons. *Nature* **447**, 1075–1080 (2007).
11. Herzfeld, D. J., Kojima, Y., Soetedjo, R. & Shadmehr, R. Encoding of action by the Purkinje cells of the cerebellum. *Nature* **526**, 439–442 (2015).
12. Lak, A., Okun, M., Moss, M. M., Gurnani, H., Farrell, K., Wells, M. J., Reddy, C. B., Kepecs, A., Harris, K. D. & Carandini, M. Dopaminergic and Prefrontal Basis of Learning from Sensory Confidence and Reward Value. *Neuron* **105**, 700–711.e6 (2020).
13. Hazra, A., Gu, F., Aulakh, A., Berridge, C., Eriksen, J. L. & Žiburkus, J. Inhibitory Neuron and Hippocampal Circuit Dysfunction in an Aged Mouse Model of Alzheimer's Disease. *PLoS ONE* **8** (ed Dickey, C. A.) e64318 (2013).
14. Busche, M. A. & Konnerth, A. Impairments of neural circuit function in Alzheimer's disease. *Philosophical Transactions of the Royal Society B: Biological Sciences* **371**, 20150429 (2016).
15. McGregor, M. M. & Nelson, A. B. Circuit Mechanisms of Parkinson's Disease. *Neuron* **101**, 1042–1056 (2019).
16. Goldberg, E. M. & Coulter, D. A. Mechanisms of epileptogenesis: a convergence on neural circuit dysfunction. *Nature Reviews Neuroscience* **14**, 337–349 (2013).

17. Houweling, A. R. & Brecht, M. Behavioural report of single neuron stimulation in somatosensory cortex. *Nature* **451**, 65–68 (2008).
18. Tanke, N., Borst, J. G. G. & Houweling, A. R. Single-Cell Stimulation in Barrel Cortex Influences Psychophysical Detection Performance. *The Journal of Neuroscience: The Official Journal of the Society for Neuroscience* **38**, 2057–2068 (2018).
19. Chettih, S. N. & Harvey, C. D. Single-neuron perturbations reveal feature-specific competition in V1. *Nature* **567**, 334–340 (2019).
20. Romo, R., Hernández, A., Zainos, A. & Salinas, E. Somatosensory discrimination based on cortical microstimulation. *Nature* **392**, 387–390 (1998).
21. Huber, D., Petreanu, L., Ghitani, N., Ranade, S., Hromádka, T., Mainen, Z. & Svoboda, K. Sparse optical microstimulation in barrel cortex drives learned behaviour in freely moving mice. *Nature* **451**, 61–64 (2008).
22. Histed, M. H. & Maunsell, J. H. R. Cortical neural populations can guide behavior by integrating inputs linearly, independent of synchrony. *Proceedings of the National Academy of Sciences* **111**, E178–E187 (2014).
23. Dagleish, H. W., Russell, L. E., Packer, A. M., Roth, A., Gauld, O. M., Greenstreet, F., Thompson, E. J. & Häusser, M. How many neurons are sufficient for perception of cortical activity? *eLife* **9** (eds Bathellier, B., Calabrese, R. L., Bathellier, B. & Carrillo-Reid, L.) e58889 (2020).
24. Gill, J. V., Lerman, G. M., Zhao, H., Stetler, B. J., Rinberg, D. & Shoham, S. Precise Holographic Manipulation of Olfactory Circuits Reveals Coding Features Determining Perceptual Detection. *Neuron* **108**, 382–393.e5 (2020).
25. Britten, K. H., Shadlen, M. N., Newsome, W. T. & Movshon, J. A. Responses of neurons in macaque MT to stochastic motion signals. *Visual Neuroscience* **10**, 1157–1169 (1993).
26. Faisal, A. A., Selen, L. P. J. & Wolpert, D. M. Noise in the nervous system. *Nature Reviews Neuroscience* **9**, 292–303 (2008).
27. Softky, W. R. & Koch, C. The highly irregular firing of cortical cells is inconsistent with temporal integration of random EPSPs. *The Journal of Neuroscience: The Official Journal of the Society for Neuroscience* **13**, 334–350 (1993).
28. Honey, C. J., Sporns, O., Cammoun, L., Gigandet, X., Thiran, J. P., Meuli, R. & Hagmann, P. Predicting human resting-state functional connectivity from structural connectivity. *Proceedings of the National Academy of Sciences* **106**, 2035–2040 (2009).
29. Musall, S., Kaufman, M. T., Juavinett, A. L., Gluf, S. & Churchland, A. K. Single-trial neural dynamics are dominated by richly varied movements. *Nature Neuroscience* **22**, 1677–1686 (2019).
30. Pons, T. P., Garraghty, P. E., Friedman, D. P. & Mishkin, M. Physiological evidence for serial processing in somatosensory cortex. *Science (New York, N.Y.)* **237**, 417–420 (1987).
31. Kamatani, D., Hishida, R., Kudoh, M. & Shibuki, K. Experience-dependent formation of activity propagation patterns at the somatosensory S1 and S2 boundary in rat cortical slices. *NeuroImage* **35**, 47–57 (2007).
32. Aronoff, R., Matyas, F., Mateo, C., Ciron, C., Schneider, B. & Petersen, C. C. H. Long-range connectivity of mouse primary somatosensory barrel cortex. *The European Journal of Neuroscience* **31**, 2221–2233 (2010).

33. Chen, J. L., Carta, S., Soldado-Magraner, J., Schneider, B. L. & Helmchen, F. Behaviour-dependent recruitment of long-range projection neurons in somatosensory cortex. *Nature* **499**, 336–340 (2013).
34. Yamashita, T., Pala, A., Pedrido, L., Kremer, Y., Welker, E. & Petersen, C. C. H. Membrane potential dynamics of neocortical projection neurons driving target-specific signals. *Neuron* **80**, 1477–1490 (2013).
35. Chen, J. L., Voigt, F. F., Javadzadeh, M., Krueppel, R. & Helmchen, F. Long-range population dynamics of anatomically defined neocortical networks. *eLife* **5** (ed King, A. J.) e14679 (2016).
36. Kwon, S. E., Yang, H., Minamisawa, G. & O'Connor, D. H. Sensory and decision-related activity propagate in a cortical feedback loop during touch perception. *Nature Neuroscience* **19**, 1243–1249 (2016).
37. Yamashita, T. & Petersen, C. C. Target-specific membrane potential dynamics of neocortical projection neurons during goal-directed behavior. *eLife* **5**, e15798 (2016).
38. Averbeck, B. B., Latham, P. E. & Pouget, A. Neural correlations, population coding and computation. *Nature Reviews Neuroscience* **7**, 358–366 (2006).
39. Kohn, A., Coen-Cagli, R., Kanitscheider, I. & Pouget, A. Correlations and Neuronal Population Information. *Annual Review of Neuroscience* **39**, 237–256 (2016).
40. Panzeri, S., Harvey, C. D., Piasini, E., Latham, P. E. & Fellin, T. Cracking the Neural Code for Sensory Perception by Combining Statistics, Intervention, and Behavior. *Neuron* **93**, 491–507 (2017).
41. Hubel, D. H. Tungsten Microelectrode for Recording from Single Units. *Science (New York, N.Y.)* **125**, 549–550 (1957).
42. McNaughton, B. L., O'Keefe, J. & Barnes, C. A. The stereotrode: A new technique for simultaneous isolation of several single units in the central nervous system from multiple unit records. *Journal of Neuroscience Methods* **8**, 391–397 (1983).
43. Buzsáki, G. Large-scale recording of neuronal ensembles. *Nature Neuroscience* **7**, 446–451 (2004).
44. Steinmetz, N. A., Aydin, C., Lebedeva, A., Okun, M., Pachitariu, M., Bauza, M., Beau, M., Bhagat, J., Böhm, C., Broux, M., Chen, S., Colonell, J., Gardner, R. J., Karsh, B., Kloosterman, F., Kostadinov, D., Mora-Lopez, C., O'Callaghan, J., Park, J., Putzeys, J., Sauerbrei, B., van Daal, R. J. J., Vollan, A. Z., Wang, S., Welkenhuysen, M., Ye, Z., Dudman, J. T., Dutta, B., Hantman, A. W., Harris, K. D., Lee, A. K., Moser, E. I., O'Keefe, J., Renart, A., Svoboda, K., Häusser, M., Haesler, S., Carandini, M. & Harris, T. D. Neuropixels 2.0: A miniaturized high-density probe for stable, long-term brain recordings. *Science* **372**, eabf4588 (2021).
45. Harris, K. D., Quijan Quiroga, R., Freeman, J. & Smith, S. Improving data quality in neuronal population recordings. *Nature neuroscience* **19**, 1165–1174 (2016).
46. Margrie, T. W., Brecht, M. & Sakmann, B. In vivo, low-resistance, whole-cell recordings from neurons in the anaesthetized and awake mammalian brain. *Pflugers Archiv: European Journal of Physiology* **444**, 491–498 (2002).
47. Houweling, A. R., Doron, G., Voigt, B. C., Herfst, L. J. & Brecht, M. Nanostimulation: manipulation of single neuron activity by juxtacellular current injection. *Journal of Neurophysiology* **103**, 1696–1704 (2010).
48. Penfield W, W. & Boldrey, E. Somatic motor and sensory representation in the cerebral cortex of man as studied by electrical stimulation. *Brain* **60**, 389–443 (1937).

49. Asanuma, H. & Sakata, H. Functional Organization of a Cortical Efferent System Examined with Focal Depth Stimulation in Cats. *Journal of Neurophysiology* **30**, 35–54 (1967).
50. Salzman, C. D., Britten, K. H. & Newsome, W. T. Cortical microstimulation influences perceptual judgements of motion direction. *Nature* **346**, 174–177 (1990).
51. Cardin, J. A., Carlén, M., Meletis, K., Knoblich, U., Zhang, F., Deisseroth, K., Tsai, L.-H. & Moore, C. I. Driving fast-spiking cells induces gamma rhythm and controls sensory responses. *Nature* **459**, 663–667 (2009).
52. Kim, C. K., Adhikari, A. & Deisseroth, K. Integration of optogenetics with complementary methodologies in systems neuroscience. *Nature Reviews Neuroscience* **18**, 222–235 (2017).
53. Grienberger, C. & Konnerth, A. Imaging calcium in neurons. *Neuron* **73**, 862–885 (2012).
54. Berridge, M. J. Neuronal calcium signaling. *Neuron* **21**, 13–26 (1998).
55. Looger, L. L. & Griesbeck, O. Genetically encoded neural activity indicators. *Current Opinion in Neurobiology*. *Neurotechnology* **22**, 18–23 (2012).
56. Chen, T.-W., Wardill, T. J., Sun, Y., Pulver, S. R., Renninger, S. L., Baohan, A., Schreiter, E. R., Kerr, R. A., Orger, M. B., Jayaraman, V., Looger, L. L., Svoboda, K. & Kim, D. S. Ultrasensitive fluorescent proteins for imaging neuronal activity. *Nature* **499**, 295–300 (2013).
57. Dana, H., Sun, Y., Mohar, B., Hulse, B. K., Kerlin, A. M., Hasseman, J. P., Tsegaye, G., Tsang, A., Wong, A., Patel, R., Macklin, J. J., Chen, Y., Konnerth, A., Jayaraman, V., Looger, L. L., Schreiter, E. R., Svoboda, K. & Kim, D. S. High-performance calcium sensors for imaging activity in neuronal populations and microcompartments. *Nature Methods* **16**, 649–657 (2019).
58. Packer, A. M., Russell, L. E., Dalgleish, H. W. P. & Häusser, M. Simultaneous all-optical manipulation and recording of neural circuit activity with cellular resolution in vivo. *Nature Methods* **12**, 140–146 (2015).
59. Huang, L., Ledochowitsch, P., Knoblich, U., Lecoq, J., Murphy, G. J., Reid, R. C., de Vries, S. E., Koch, C., Zeng, H., Buice, M. A., Waters, J. & Li, L. Relationship between simultaneously recorded spiking activity and fluorescence signal in GCaMP6 transgenic mice. *eLife* **10** (eds Westbrook, G. L., Svoboda, K., Higley, M. & Sabatini, B. L.) e51675 (2021).
60. Andermann, M. L., Gilfoy, N. B., Goldey, G. J., Sachdev, R. N. S., Wölfel, M., McCormick, D. A., Reid, R. C. & Levene, M. J. Chronic Cellular Imaging of Entire Cortical Columns in Awake Mice Using Microprisms. *Neuron* **80**, 900–913 (2013).
61. Lichtman, J. W. & Conchello, J.-A. Fluorescence microscopy. *Nature Methods* **2**, 910–919 (2005).
62. Nwaneshiudu, A., Kuschal, C., Sakamoto, F. H., Anderson, R. R., Schwarzenberger, K. & Young, R. C. Introduction to confocal microscopy. *Journal of Investigative Dermatology* **132**, 1–5 (2012).
63. Helmchen, F. & Denk, W. Deep tissue two-photon microscopy. *Nature Methods* **2**, 932–940 (2005).
64. Helmchen, F., Svoboda, K., Denk, W. & Tank, D. W. In vivo dendritic calcium dynamics in deep-layer cortical pyramidal neurons. *Nature Neuroscience* **2**, 989–996 (1999).

65. Stosiek, C., Garaschuk, O., Holthoff, K. & Konnerth, A. In vivo two-photon calcium imaging of neuronal networks. *Proceedings of the National Academy of Sciences* **100**, 7319–7324 (2003).
66. Lütcke, H., Margolis, D. J. & Helmchen, F. Steady or changing? Long-term monitoring of neuronal population activity. *Trends in Neurosciences* **36**, 375–384 (2013).
67. Driscoll, L. N., Pettit, N. L., Minderer, M., Chettih, S. N. & Harvey, C. D. Dynamic Reorganization of Neuronal Activity Patterns in Parietal Cortex. *Cell* **170**, 986–999.e16 (2017).
68. Miesenbock, G. The Optogenetic Catechism. *Science* **326**, 395–399 (2009).
69. Deisseroth, K. Optogenetics. *Nature Methods* **8**, 26–29 (2011).
70. Zhang, F., Gradinaru, V., Adamantidis, A. R., Durand, R., Airan, R. D., de Lecea, L. & Deisseroth, K. Optogenetic interrogation of neural circuits: technology for probing mammalian brain structures. *Nature Protocols* **5**, 439–456 (2010).
71. Tye, K. M., Mirzabekov, J. J., Warden, M. R., Ferenczi, E. A., Tsai, H.-C., Finkelstein, J., Kim, S.-Y., Adhikari, A., Thompson, K. R., Andalman, A. S., Gunaydin, L. A., Witten, I. B. & Deisseroth, K. Dopamine neurons modulate neural encoding and expression of depression-related behaviour. *Nature* **493**, 537–541 (2013).
72. Zalocusky, K. A., Ramakrishnan, C., Lerner, T. N., Davidson, T. J., Knutson, B. & Deisseroth, K. Nucleus accumbens D2R cells signal prior outcomes and control risky decision-making. *Nature* **531**, 642–646 (2016).
73. Mattis, J., Brill, J., Evans, S., Lerner, T. N., Davidson, T. J., Hyun, M., Ramakrishnan, C., Deisseroth, K. & Huguenard, J. R. Frequency-Dependent, Cell Type-Divergent Signaling in the Hippocamposeptal Projection. *Journal of Neuroscience* **34**, 11769–11780 (2014).
74. Tye, K. M., Prakash, R., Kim, S.-Y., Fenno, L. E., Grosenick, L., Zarabi, H., Thompson, K. R., Gradinaru, V., Ramakrishnan, C. & Deisseroth, K. Amygdala circuitry mediating reversible and bidirectional control of anxiety. *Nature* **471**, 358–362 (2011).
75. Krook-Magnuson, E., Armstrong, C., Oijala, M. & Soltesz, I. On-demand optogenetic control of spontaneous seizures in temporal lobe epilepsy. *Nature Communications* **4**, 1376 (2013).
76. Olshausen, B. A. & Field, D. J. Sparse coding of sensory inputs. *Current Opinion in Neurobiology* **14**, 481–487 (2004).
77. Yizhar, O., Fenno, L. E., Prigge, M., Schneider, F., Davidson, T. J., O'Shea, D. J., Sohal, V. S., Goshen, I., Finkelstein, J., Paz, J. T., Stehfest, K., Fudim, R., Ramakrishnan, C., Huguenard, J. R., Hegemann, P. & Deisseroth, K. Neocortical excitation/inhibition balance in information processing and social dysfunction. *Nature* **477**, 171–178 (2011).
78. Mardinaly, A. R., Oldenburg, I. A., Pégard, N. C., Sridharan, S., Lyall, E. H., Chesnov, K., Brohawn, S. G., Waller, L. & Adesnik, H. Precise multimodal optical control of neural ensemble activity. *Nature Neuroscience* **21**, 881–893 (2018).
79. Marshel, J. H., Kim, Y. S., Machado, T. A., Quirin, S., Benson, B., Kadmon, J., Raja, C., Chibukhchyan, A., Ramakrishnan, C., Inoue, M., Shane, J. C., McKnight, D. J., Yoshizawa, S., Kato, H. E., Ganguli, S. & Deisseroth, K. Cortical

- layer-specific critical dynamics triggering perception. *Science (New York, N.Y.)* **365**, eaaw5202 (2019).
- 80. Peirson, S. N., Brown, L. A., Pothecary, C. A., Benson, L. A. & Fisk, A. S. Light and the laboratory mouse. *Journal of Neuroscience Methods* **300**, 26–36 (2018).
 - 81. Russell, L. E., Yang, Z., Tan, P. L., Fişek, M., Packer, A. M., Dalgleish, H. W., Chettih, S., Harvey, C. D. & Häusser, M. The influence of visual cortex on perception is modulated by behavioural state. *bioRxiv* (2019).
 - 82. Daie, K., Svoboda, K. & Druckmann, S. Targeted photostimulation uncovers circuit motifs supporting short-term memory. *Nature Neuroscience* **24**, 259–265 (2021).
 - 83. Friedrich, J., Zhou, P. & Paninski, L. Fast online deconvolution of calcium imaging data. *PLOS Computational Biology* **13**, e1005423 (2017).
 - 84. Shaw, P. J. & Rawlins, D. J. The point-spread function of a confocal microscope: its measurement and use in deconvolution of 3-D data. *Journal of Microscopy* **163**, 151–165 (1991).
 - 85. Gerchberg, R. & Saxton, W. A Practical Algorithm for the Determination of Phase from Image and Diffraction Plane Pictures. *Optik Vol.* **35**, 237–246 (1972).
 - 86. Watson, B. O., Yuste, R. & Packer, A. M. PackIO and EphysViewer: software tools for acquisition and analysis of neuroscience data. *bioRxiv*, 054080 (2016).
 - 87. Akam, T., Lustig, A., Rowland, J., Kapanaiah, S. K. T., Esteve-Agraz, J., Panniello, M., Marquez, C., Kohl, M., Kätzel, D., Costa, R. M. & Walton, M. pyControl: Open source, Python based, hardware and software for controlling behavioural neuroscience experiments. *bioRxiv*, 2021.02.22.432227 (2021).
 - 88. Brophy, A. L. Alternatives to a table of criterion values in signal detection theory. *Behavior Research Methods, Instruments, & Computers* **18**, 285–286 (1986).
 - 89. Pedregosa, F., Varoquaux, G., Gramfort, A., Michel, V., Thirion, B., Grisel, O., Blondel, M., Prettenhofer, P., Weiss, R., Dubourg, V., Vanderplas, J., Passos, A. & Cournapeau, D. Scikit-learn: Machine Learning in Python. *arXiv*, 6 (2012).